A generalized mechano-statistical transient network model for unravelling the network topology and elasticity of hydrophobically associating multiblock copolymers in aqueous solutions

Macromolecules

pubs.acs.org/Macromolecules Article

A Generalized Mechano-statistical Transient Network Model for Unravelling the Network Topology and Elasticity of Hydrophobically Associating Multiblock Copolymers in Aqueous Solutions

An-Sofie Huysecom, Wim Thielemans, Paula Moldenaers, and Ruth Cardinaels*

Cite This: *Macromolecules* 2023, 56, 612−633 Read Online

ACCESS | Metrics & More | Article Recommendations | Supporting Information

ABSTRACT: In this contribution, we unravel the transient network topology and elasticity of micellar networks formed by hydrophobically associating multiblock copolymers in aqueous solutions. Unlike studies on conventional triblock copolymers bearing hydrophobic blocks as end groups, our research focuses on alternating poly(ethylene oxide) (PEO) and poly(propylene oxide) (PPO) multiblock copolymers having multiple hydrophobic PPO blocks along the chain. We adopt a combinatorics approach to extend and generalize the mechano-statistical transient network model developed by Annable et al. for telechelic triblock copolymers [*Journal of Rheology*, **1993**, *37*, 695] to multiblock copolymers. The model allows one to predict the concentration dependent elasticity of networks formed by multiblock copolymers with known molecular characteristics by using knowledge of the micellar network microstructure. The spatial distribution of the hydrophobic nodes is inferred from Small-Angle X-ray Scattering (SAXS) by converting the structure factor to the radial distribution function. The number of closely neighboring micellar cores between which an elastic bridge can be formed (n_m) is calculated by spherical integration of the radial distribution function up to a distance of the radius of gyration of an intermediate soluble PEO block. Using the evolution of n_m with concentration as an input for the model, the predictions show good agreement with experimental elasticity data, as inferred from the plateau modulus in linear shear rheology. The network evolves from loop-dominated, poorly elastic with cross-linking nodes with low functionality at low concentrations to bridge-dominated, highly elastic with higher node functionalities at more elevated concentrations. It is anticipated that our generalized mechano-statistical transient network model can also be used for equally spaced, multisticker associating polymers forming networks by multifunctional interactions other than micellar aggregation.

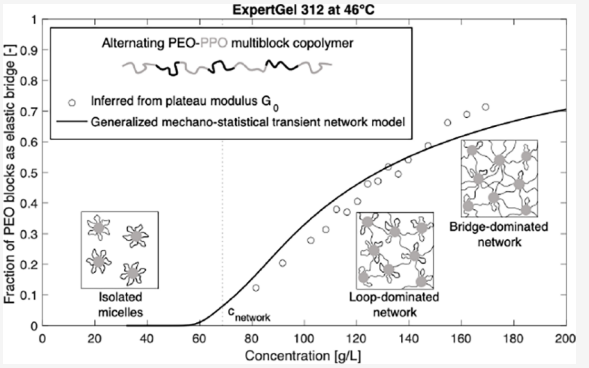

1. INTRODUCTION

In recent years, physical polymer gels have received a great deal of attention not only from material scientists for the development of novel, custom-made materials for different applications but also from polymer physicists to unravel fundamental polymer principles. Such physical gels are formed by macromolecules containing "sticky" groups, which undergo transient noncovalent interactions and form the cross-linking nodes of a 3-dimensional, sample spanning polymer network restricting flow. Different physical interactions, such as hydrogen bonding,[1−5] ionic interactions,[6−8] metal−ligand complexation,[9−11] and inclusion complexation[12,13] have been employed in physical hydrogels. The final gel topology, mechanical properties, and dynamics are not only determined by the strength and functionality of the interactions but are also affected by the location of the sticky groups, either as telechelic end groups or along the polymer backbone. An overview of the formation, structure, dynamics, and mechanical properties of supramolecular polymer networks and gels can be found in the review paper by Seiffert and Sprakel.[14] The transient character of the physical cross-links delivers properties in between those of entangled polymer solutions and those of permanently cross-linked, chemical gels. It also provides the networks with excellent self-healing,[15−17] stimuli-responsive,[18,19] and shape-memory[3,20] properties. Therefore, physical polymer gels have proven to be useful in a plethora of advanced applications including microfluidics,[21] superabsorbents,[22] (bio)sensors,[23] and artificial muscles.[24]

A particularly interesting type of interaction is found in block copolymers consisting of hydrophilic (A) and hydrophobic (B) blocks. In aqueous solutions, the hydrophobic blocks sponta-

Received: July 19, 2022
Revised: November 28, 2022
Published: January 2, 2023

https://doi.org/10.1021/acs.macromol.2c01500
Macromolecules 2023, 56, 612−633

neously undergo phase separation due to the entropically driven hydrophobic effect, resulting in micellar assemblies.[25,26] At low concentrations, isolated micelles consisting of a hydrophobic core stabilized by a hydrophilic corona are formed. At more elevated concentrations, an elastic gel can be formed depending on the molecular architecture of the block copolymers.[27] Diblock copolymers as well as ABA and BAB triblock copolymers have often been used as model systems to study physical gels formed by hydrophobic association, but the underlying mechanisms of gel formation are fundamentally different. The hairy micelles composed of AB diblock or ABA triblock copolymers jam together in crystalline lattices forming a gel at elevated concentrations.[28−30] On the other hand, BAB triblock copolymers form so-called flowerlike micelles with hydrophilic loops. At higher concentrations, the intermediate hydrophilic A blocks have the potential to form an elastic bridge in between two separate micellar cores, thereby resulting in a sample spanning polymer network.[31−35] Micellar gels based on block copolymers are of particular interest in biomedical applications[36] as drug delivery systems[37,38] and tissue engineering scaffolds[39−42] or for improved wound healing.[43] In this regard, the presence of small hydrophobic domains allows efficient encapsulation,[44] controlled release,[45,46] and targeted delivery[47] of therapeutic agents such as pharmaceutical drugs, proteins, or (stem) cells. Knowledge of the sizes, spatial arrangement, and interconnectivity of the domains is crucial in understanding and efficiently designing micellar gels with tailored mechanical properties. Well-known examples of nonionic ABA triblock copolymers are poloxamers, consisting of poly(ethylene oxide) (PEO) and poly(propylene oxide) (PPO) blocks. Such PEO_x−PPO_y−PEO_x triblock copolymers are commercially available as Pluronics with different PEO (x) and PPO (y) block lengths.[48] Due to the dehydration of the PPO block at temperatures exceeding 15 °C,[49,50] aqueous solutions of poloxamers have a Critical Micelle Temperature (CMT) and a Critical Micelle Concentration (CMC), above which micellar aggregation occurs. Governed by the ratio of PPO to PEO as well as the overall molecular weight, they exhibit interesting phase behavior with a rich polymorphism, ranging from isotropic polymer solutions, over micellar solutions to cubic, hexagonal and lamellar lyotropic liquid crystalline phases upon increasing concentration and/or temperature.[49,50] Their excellent biocompatibility and nontoxicity, together with their thermoreversible gelation from a easily injectable sol at room temperature to an elastic micellar gel at human body temperature, make Pluronics one of the most widely used hydrophobically associating copolymers in hydrogels for (bio)medical applications.[51,52]

During the last few decades, many authors have tried to fundamentally understand and predict the linear and nonlinear rheological properties of supramolecular polymer networks and gels based on so-called transient network models. In this regard, the transient network models originally developed by Green and Tobolsky,[53] Yamamoto,[54] and Lodge,[55] and later modified by Tanaka and Edwards[56−59] for unentangled telechelic, physically associating polymers, form the basis for more generalized constitutive modeling which captures complex nonlinear features such as shear thinning and thickening,[60−62] thereby making use of observations from Brownian dynamics simulations of such transient networks.[63] An important model system of telechelic polymers used for the experimental verification of transient network models, are hydrophobically modified urethane−ethoxylate (HEUR) polymers consisting of hydrophilic PEO end-capped by hydrophobic groups such as aliphatic alcohols using urethane bonds. They thus represent BAB triblock copolymers and generally form a bridged micellar gel at elevated concentrations. Aqueous solutions of HEUR have been studied extensively by both linear and nonlinear rheology and compared to the predictions from transient network models.[62,64−66] Their linear rheological response follows the ideal Maxwell model, facilitating the extraction of the plateau modulus and one characteristic relaxation time, fully governed by the dissociation of the junctions and hence of the order of the bond lifetime.[64] Whereas constitutive modeling accurately describes many features of the linear and nonlinear rheological behavior of transient networks, it fails to explain the strong effect of concentration on the network's rheological properties.[67] Therefore, a different approach as compared to constitutive modeling was taken by Annable et al., who developed a so-called mechano-statistical transient network model for unentangled, telechelic BAB triblock copolymers.[67,68] Based on the probabilities of the intermediate A block of either forming a loop or a bridge, they predict a topological evolution from loop-dominated to bridge-dominated upon increasing concentration, which is responsible for the macroscopic mechanical behavior. Their fairly simple approach resulted in accurate predictions of the evolution of the number density of elastically active chains for HEUR polymers, as inferred from linear shear rheology, and showed agreement with their predictions from simplified Monte Carlo simulations.[67]

Unlike telechelic polymers exhibiting ideal Maxwellian behavior, nontelechelic associative polymers, having "sticky" groups distributed along the chain, show more complex linear rheological behavior.[27,69] A limited amount of studies try to capture their rheological response based on constitutive modeling exhibiting only qualitative agreement with experimental data,[70−72] while simulations usually succeed in predicting the response more accurately but lack an a priori physical interpretation of the system's behavior.[73,74] Additionally, different theoretical frameworks to predict scaling relations for rheological properties such as the viscosity, elastic modulus and relaxation times with concentration, have been developed by Leibler, Rubinstein, and Semenov. In this regard, the sticky Rouse[75,76] and sticky reptation[77,78] models for unentangled and entangled multisticker associative polymer solutions were developed based on a single-chain approach with pairwise interactions between sticky groups. Despite the extensive theoretical background of these "sticky" models, experimental rheological data often show limited agreement with the model predictions.[79−82] Moreover, most associative polymer solutions obeying similar scaling relations as predicted by the "sticky" frameworks almost never fulfill the assumption of simple pairwise association.[83−85] Alternatively, transient networks with cross-linking nodes formed by large-scale aggregates of sticky (end)groups were treated by Semenov et al. according to a collective approach, in which the dynamics of the overall aggregate assembly dominate over single chain relaxations.[86,87] However, recent NMR experiments by Mordvinkin et al. on telechelically associating polymers have shown that also for networks formed by large, micellar cross-linking nodes, the relaxation is governed by single chain relaxation principles rather than micellar reorganization.[88,89] In summary, the lack of quantitative agreement between theoretical frameworks and experimental data, as well as the lack of a qualitative agreement between different model approaches, indicates that a thorough understanding of the rheological behavior of networks formed

https://doi.org/10.1021/acs.macromol.2c01500
Macromolecules 2023, 56, 612−633

Table 1. Example of the Combinatorics Approach for a Chain with $a = 4$ Associating Blocks (Represented as ●) and $a - 1 = 3$ Soluble Blocks (Represented as a Bridge or Loop), Possible Configurations and the Resulting Probabilities, the Average Number of Associating Blocks in one Cross-Linking Node (Represented as ○), and the Average Number of Bridges Connected to one Cross-Linking Node[a]

	Configuration	Configuration probability	Overall configuration probability for i bridges	Average amount of bridges connected to one crosslinking node	Average amount of associating blocks in a crosslinking node
i = 0		$F_1^0 \cdot F_2^3$	$\binom{3}{0} \cdot F_1^0 \cdot F_2^3$	0	4
			$\binom{3}{0} = \frac{3!}{0!(3-0)!} = 1$	$= 0/1$	$= 4/1$
i = 1		$F_1^1 \cdot F_2^2$	$\binom{3}{1} \cdot F_1^1 \cdot F_2^2$	$\frac{1}{2} \cdot 1 + \frac{1}{2} \cdot 1$	$\frac{1}{2} \cdot 2 + \frac{1}{2} \cdot 2$
		$F_1^1 \cdot F_2^2$		$\frac{1}{2} \cdot 1 + \frac{1}{2} \cdot 1$	$\frac{1}{2} \cdot 3 + \frac{1}{2} \cdot 1$
		$F_1^1 \cdot F_2^2$		$\frac{1}{2} \cdot 1 + \frac{1}{2} \cdot 1$	$\frac{1}{2} \cdot 1 + \frac{1}{2} \cdot 3$
			$\binom{3}{1} = \frac{3!}{1!(3-1)!} = 3$	$= 2/2$	$= 4/2$
i = 2		$F_1^2 \cdot F_2^1$	$\binom{3}{2} \cdot F_1^2 \cdot F_2^1$	$\frac{1}{3} \cdot 1 + \frac{1}{3} \cdot 2 + \frac{1}{3} \cdot 1$	$\frac{1}{3} \cdot 1 + \frac{1}{3} \cdot 2 + \frac{1}{3} \cdot 1$
		$F_1^2 \cdot F_2^1$		$\frac{1}{3} \cdot 1 + \frac{1}{3} \cdot 2 + \frac{1}{3} \cdot 1$	$\frac{1}{3} \cdot 2 + \frac{1}{3} \cdot 1 + \frac{1}{3} \cdot 1$
		$F_1^2 \cdot F_2^1$		$\frac{1}{3} \cdot 1 + \frac{1}{3} \cdot 2 + \frac{1}{3} \cdot 1$	$\frac{1}{3} \cdot 1 + \frac{1}{3} \cdot 1 + \frac{1}{3} \cdot 2$
			$\binom{3}{2} = \frac{3!}{2!(3-2)!} = 3$	$= 4/3$	$= 4/3$
i = 3		$F_1^3 \cdot F_2^0$	$\binom{3}{3} \cdot F_1^3 \cdot F_2^0$	$\frac{2}{4} \cdot 1 + \frac{2}{4} \cdot 2$	1
			$\binom{3}{3} = \frac{3!}{3!(3-3)!} = 1$	$= 6/4$	$= 4/4$
$\sum_{i=0}^{a-1}$	2^{a-1}	$F_1^i \cdot F_2^{a-1-i}$	$\binom{a-1}{i} \cdot F_1^i \cdot F_2^{a-1-i}$	$\frac{2(i+1)-2}{i+1}$	$\frac{a}{i+1}$

[a]The last row in gray shows the symbolic expressions.

by nontelechelic associative polymer solutions remains an open question.

Therefore, the goal of our study is to extend Annable's mechano-statistical approach, developed for linear elasticity of telechelic unentangled associative polymers, to multisticker unentangled associative polymers using combinatorics. This approach might open up a different perspective on transient networks formed by nontelechelic associative polymers, as it allows one to gain insights in the probabilities of soluble blocks to form loops or bridges, in the functionalities of the cross-linking nodes as well as in the evolution of the number of elastically active bridges, all as a function of concentration. Besides the molecular characteristics of the multisticker polymer chains, in-depth knowledge of the microstructure of the transient network is crucial for understanding the final mechanical properties of physical gels formed by micellar aggregation. In this work, we will use Small-Angle X-ray Scattering (SAXS) to determine the relevant length scales, the aggregation numbers, and the overall spatial distribution of the micellar nodes in thermoreversible transient networks formed by alternating PEO−PPO multiblock copolymers in aqueous solutions. By combining knowledge about the network topology with our mechano-statistical model, we can detect micro-structural changes as a function of concentration and how they translate into macroscopic behavior. The performance of the transient network model is verified by comparing the model results with the evolution of the number density of elastically active chains with concentration as inferred from linear shear rheology.

2. GENERALIZED MECHANO-STATISTICAL TRANSIENT NETWORK MODEL

In this section, the mechano-statistical transient network model originally developed by T. Annable and co-workers for HEUR copolymers bearing their associating groups as telechelic end groups[67,68] is extended and generalized for alternating multi-

https://doi.org/10.1021/acs.macromol.2c01500
Macromolecules 2023, 56, 612−633

block copolymers. The presence of more than two associating blocks along the chain significantly increases the amount of possible configurations of the chain as compared to those of telechelic polymers and hence also the complexity of the model. Here, the Annable model is extended by adopting a combinatorics approach for all possible configurations of the multiblock copolymers. In what follows, this approach and the derivation of the expression predicting the amount of elastically active chains as a function of concentration is discussed. The simplest case of our model framework, i.e., that of triblock copolymers having telechelic associating groups, is treated in the Supporting Information and results in the original expressions as derived by Annable et al.[67,68]

Consider a linear block copolymer chain with a associating blocks, of which 2 are telechelic and the other $a-2$ are evenly distributed along the chain. As a consequence, the chain contains $a-1$ soluble blocks which are capped by associating blocks. In fact, it can be noted that the assumption of associating end blocks is not a limitation of the model, since soluble end blocks form dangling ends that do not contribute to the network's elasticity. In this regard, it is also important to stress that entanglements are not taken into account in this transient network model, which aims at unentangled polymers. The absence of entanglements will be experimentally confirmed for our multiblock copolymers in Section 4.1. Since block copolymers form micellar assemblies with large aggregation numbers N_{agg} (often $N_{agg} \gg 10$ for self-assembly of nonionic block copolymers[26]), the association interaction between the associating blocks is assumed to be multifunctional ($f > 2$) in the following framework. The model is thus expected to apply not only to systems interacting through micellar aggregation but also to polymer chains bearing smaller associating groups along their backbone or as a side group, which form multifunctional interaction nodes. In this regard, an interesting review by Seiffert and co-workers reveals the importance of such junction clustering in polymer networks constructed through physical, supramolecular interactions.[90] Since transient micellar networks are only formed at concentrations well above the CMC, the concentration of free unimers is assumed to be negligible in our model derivations.

2.1. Configuration Probabilities. Each of the $a-1$ capped soluble blocks is presumed to have only two possible configurations. It either forms a bridge in between two different association nodes, or it forms a loop connected to just one association node. This assumption can be justified by the large binding energy between the associating blocks,[67] resulting in a negligible fraction of associating blocks being present as either free dangling ends or as entire freely soluble chains, both configurations not contributing to an association node. The amount of possible configurations for a chain with $a-1$ capped soluble blocks thus equals 2^{a-1}. As an example, the second column in Table 1 shows the 8 possible configurations for a chain with $a = 4$ associating blocks and $a - 1 = 3$ capped soluble blocks. Importantly, it is assumed that once a chain leaves a certain association node to form a bridge toward another node, it eventually does not come back to that same node. Chain configurations with so-called redundant bridges in between the same association nodes, might be possible for chains with $a \geq 3$ and for configurations having $i \geq 2$ bridges, and they are expected to be more significantly present in long multiblock copolymers with $a \gg 3$. Therefore, the performance of our model is anticipated to be insufficient for systems in which such configurations are predominant, and adjustments might be needed.

Following the terminology from the original work by Annable,[67] the probability of a capped soluble block to from a bridge is denoted as F_1. Assuming a negligible fraction of "open" stickers, the probability of forming a loop F_2 is equal to $1 - F_1$. The probability of a specific configuration with i bridges and hence $a - 1 - i$ loops thus equals $F_1^{\,i} \cdot F_2^{\,a-1-i}$. Note that multiple configurations having i bridges exist due to the possibility of a different order of occurrence of the bridges and loops, as shown in Table 1. The total amount of configurations with i bridges can be calculated from the binomial coefficient

$$\binom{a-1}{i} = \frac{a-1!}{i!\quad (a-1-i)!} \tag{1}$$

Hence, the overall probability of all configurations with i bridges and $a-1-i$ loops is

$$\binom{a-1}{i} \cdot F_1^{\,i} \cdot F_2^{\,a-1-i} \tag{2}$$

as illustrated in the fourth column in Table 1.

In micellar networks formed by soluble polymer bridges, there usually exists a critical onset concentration for network formation $c_{network}$. At dilute concentrations below this $c_{network}$, the nearest neighboring micellar cores are all too far away for an intermediate hydrophilic block to span the distance between them and hence to form a bridge. The resulting structure at concentrations below $c_{network}$ is thus a purely viscous solution of isolated micelles, as can be seen in Figure 1. Therefore, the probability of forming a loop F_2 should equal 1 below $c_{network}$. At concentrations above $c_{network}$, other micellar cores appear within the volume spanned by a soluble block, such that bridges toward other micellar cores can arise. These bridges provide the network with its elasticity, while the dynamic, reversible character of the association interaction gives rise to so-called transient cross-linking nodes by continuous association and dissociation events. Figure 1 schematically illustrates the transition from a dilute micellar solution toward a transient elastic network at concentrations above $c_{network}$.

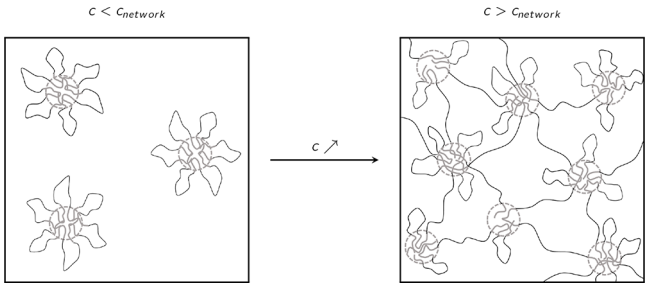

Figure 1. Transition from a dilute solution of isolated flowerlike micelles to a transient network of bridged micellar cores at concentrations above the critical network concentration ($c_{network}$).

In this work, we will replicate Annable's crucial approximation that the probability of forming a loop F_2 is inversely proportional to the average amount of association (micellar) nodes n_m, present in the volume defined by the span of a soluble block.[67,68] This n_m thus represents the amount of micellar nodes in such close proximity that a soluble block can possibly form a bridge in between these nodes. Note that below $c_{network}$, only one micellar core is present within the volume defined by the soluble blocks

https://doi.org/10.1021/acs.macromol.2c01500
Macromolecules 2023, 56, 612−633

($n_m = 1$), and the probability of forming a loop $F_2 = 1/n_m$ thus equals 1.

2.2. Node Functionality. Since the amount of bridges is crucial for the network elasticity, we define an average node functionality $\langle\Psi\rangle$ as the average amount of bridges that originate from an association node. This average functionality can be calculated as the product of N_b, the average amount of bridges one chain contributes to a cross-linking node [bridges/chain], and N_c, the average amount of chains contributing to one cross-linking node [chains/node]. The latter can be approximated as N_{agg}/N_a, in which N_{agg} is the aggregation number of the micellar node, i.e., the amount of hydrophobic blocks per micellar core [associating blocks/node], and N_a is the average amount of associating blocks one chain contributes to a cross-linking node [associating blocks/chain]. Both N_b and N_a can be calculated from a summation over all possible configurations, resulting in the following expressions:

$$N_b = \sum_{i=0}^{a-1} \underbrace{\frac{2(i+1)-2}{i+1}}_{\substack{\text{average \# of bridges}\\ \text{a chain with i bridges}\\ \text{contributes to a node}}} \cdot \underbrace{\binom{a-1}{i} \cdot F_1^i \cdot F_2^{a-1-i}}_{\substack{\text{overall probability of}\\ \text{having a chain}\\ \text{with i bridges}}} \tag{3}$$

$$N_a = \sum_{i=0}^{a-1} \underbrace{\frac{a}{i+1}}_{\substack{\text{average \# of}\\ \text{associating blocks}\\ \text{a chain with i bridges}\\ \text{contributes to a node}}} \cdot \underbrace{\binom{a-1}{i} \cdot F_1^i \cdot F_2^{a-1-i}}_{\substack{\text{overall probability of}\\ \text{having a chain}\\ \text{with i bridges}}} \tag{4}$$

An illustrative example of the calculation of the factors in the expressions for N_b and N_a is shown in the last two columns of Table 1 for a multiblock copolymer with 4 associating blocks. The final expression of $\langle\Psi\rangle$ is shown in eq 5:

$$\langle\Psi\rangle = N_b \cdot N_c = N_b \cdot \frac{N_{agg}}{N_a} = N_{agg} \cdot \frac{\sum_{i=0}^{a-1} \frac{2(i+1)-2}{i+1} \cdot \binom{a-1}{i} \cdot F_1^i \cdot F_2^{a-1-i}}{\sum_{i=0}^{a-1} \binom{a}{i+1} \cdot F_1^i \cdot F_2^{a-1-i}} \tag{5}$$

The association nodes exhibit a distribution of functionalities defined by the probability distribution function $P(\Psi)$, i.e., the probability P of finding a node with a certain functionality Ψ. This distribution does not only arise from fluctuations in the functionality itself at a constant aggregation number but also can be partly attributed to micellar polydispersity (at a constant temperature and concentration) resulting in fluctuations in aggregation number.[67] The functionality distribution is assumed to be binomial around the average value $\langle\Psi\rangle$ determined in eq 5, with the maximum functionality Ψ_{max} attained when all $a - 1$ capped soluble blocks form bridges ($F_1 = 1$). The expressions for $P(\Psi)$ and Ψ_{max} are given in eqs 6 and 7, respectively:

$$P(\Psi) = \binom{\Psi_{max}}{\Psi} \cdot \left(\frac{\langle\Psi\rangle}{\Psi_{max}}\right)^{\Psi} \cdot \left(1 - \frac{\langle\Psi\rangle}{\Psi_{max}}\right)^{\Psi_{max}-\Psi} \tag{6}$$

$$\Psi_{max} = \langle\Psi\rangle\Big|_{F_1=1} = N_{agg} \cdot \frac{2a-2}{a} \tag{7}$$

Even though no fundamental basis for assuming a binomial distribution of node functionalities exists, two physical limitations justify our choice of the distribution function: (1) the function should be discrete, and (2) the function should be delimited in nature as $\Psi \in \{0, 1, 2, ..., \Psi_{max}\}$. It can be noted that the definition of Ψ_{max} in eq 7 does not necessarily result in a discrete number, and therefore, it is approximated as its nearest natural number. As expected, for multiblock copolymers with $a > 2$, the Ψ_{max} value will exceed N_{agg} due to the fact that when $F_1 = 1$, each nontelechelic associating block will create 2 bridges leaving the same node.

2.3. Elastically Active Bridges. Since loops are assumed to be elastically inactive, the number density of elastically active chains (ν) can be calculated from the amount of bridges connected to a node multiplied by the number density of nodes (n_{mic}). For this calculation, a few considerations must be made. First, a bridge connects two cross-linking nodes and hence, each bridge included in the node functionality Ψ only counts as half of an elastically active chain. Therefore, the amount of elastically active chains involves the summation of the node functionalities divided by 2 ($\Psi/2$), weighted with their occurrence probability ($P(\Psi)$). Second, only node functionalities $\Psi \geq 3$ should be taken into account in the calculation of unique elastically active chains, since nodes with $\Psi = 1$ are dangling ends not contributing to a sample-spanning connectivity, while nodes with $\Psi = 2$ act as additional, redundant steps in dangling ends, and in superloops or superbridges consisting of multiple connected nodes. Schematic illustrations of a dangling end, a superloop and a superbridge can be found in Figure 2. Lastly, the

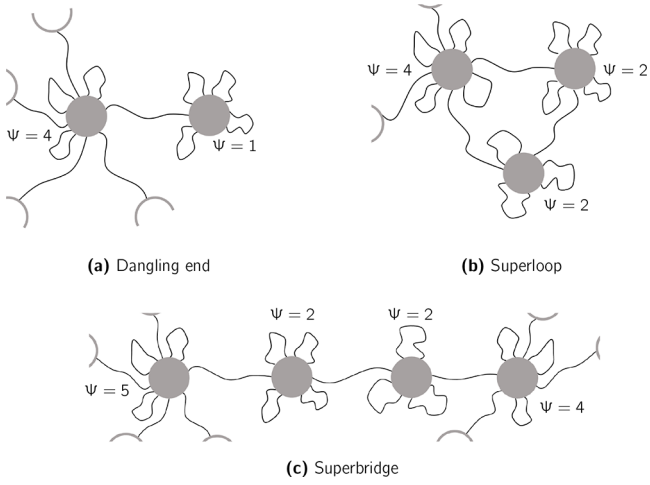

Figure 2. Schematic illustrations of (a) a dangling end, (b) a superloop, and (c) a superbridge. For simplicity, the micellar cores are represented as filled gray circles. The node functionalities Ψ of the involved cores are indicated on the figures.

fraction of bridges originating from a node with $\Psi \geq 3$, which are linked to a unifunctional node, should also be eliminated in the expression for the number density of elastically active chains. Accordingly, only a fraction $(1 - P(0) - P(1))/(1 - P(0))$ of the summation is included in eq 8. The denominator contains $1 - P(0)$ instead of 1 because each bridge must connect to a node with a functionality of 1 or more (zero-functional nodes ($\Psi = 0$) only have loops).

$$\nu = n_{mic} \cdot \left(\frac{1 - P(0) - P(1)}{1 - P(0)}\right) \cdot \sum_{\Psi=3}^{\Psi_{max}} \left(\frac{\Psi}{2}\right) \cdot P(\Psi) \tag{8}$$

https://doi.org/10.1021/acs.macromol.2c01500
Macromolecules 2023, 56, 612−633

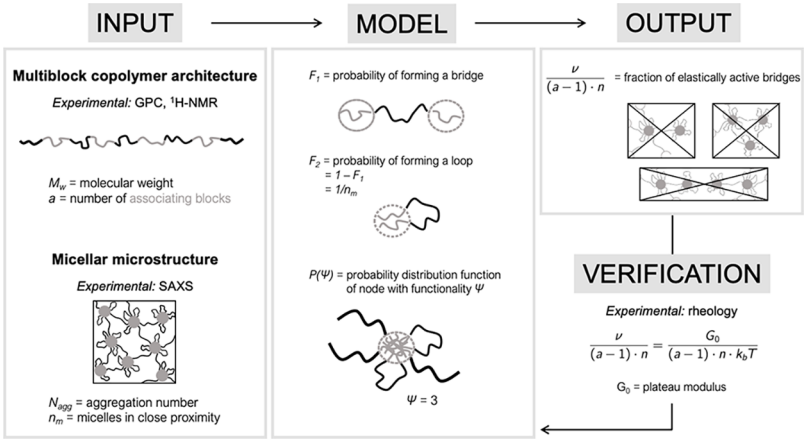

Figure 3. Schematic overview of the transient network model: input, model principles, output, and model verification. The experimental methods are also included.

The number density of micelles n_{mic} can be calculated from the number density of chains n, the aggregation number N_{agg} and the number of associating blocks a, as shown in eq 9:

$$n_{mic} = \frac{n\cdot a}{N_{agg}} \tag{9}$$

The number density of chains n can be linked to the mass concentration c of multiblock copolymer in solution by making use of its molecular weight M_w and Avogadro's number N_{Av} (6.02×10^{-23} mol^{-1}). Equation 10 thus represents the evolution of the number density of elastically active chains as a function of concentration:

$$\nu = \left(\frac{c\cdot N_{Av}}{M_w}\cdot\frac{a}{N_{agg}}\right)\cdot\left(\frac{1 - P(0) - P(1)}{1 - P(0)}\right)\cdot\sum_{\Psi=3}^{\Psi_{max}}\left(\frac{\Psi}{2}\right)\cdot P(\Psi) \tag{10}$$

Note that this equation can be fully evaluated, without the need for parameter fitting, by knowledge of a, M_w, N_{agg}, and n_m. The latter reveals its importance in the calculation of the bridge and loop probabilities F_1 and F_2, respectively, and is eventually reflected in the node functionality distribution function $P(\Psi)$ around the average value $\langle\Psi\rangle$. Equation 10 allows one to calculate the fraction of all $(a-1)\cdot n$ available soluble blocks, which are effectively active as unique elastic bridges according to eq 11:

$$\frac{\nu}{(a-1)\cdot n} = \left(\frac{a}{(a-1)\cdot N_{agg}}\right)\cdot\left(\frac{1 - P(0) - P(1)}{1 - P(0)}\right)\cdot\sum_{\Psi=3}^{\Psi_{max}}\left(\frac{\Psi}{2}\right)\cdot P(\Psi) \tag{11}$$

The performance of this model prediction can be verified by comparing the model expression of the number density of elastically active chains with the information as extracted from rheological measurements in the linear viscoelastic region (see Section 4.3). Analogous to the affine network theory of rubber elasticity,[91] ν can be estimated from the plateau modulus G_0, i.e., the constant elastic modulus G' usually detected at high frequencies for viscoelastic networks, as

$$\nu = \frac{G_0}{k_b\cdot T} \tag{12}$$

in which k_b is the Boltzmann constant (1.38×10^{-23} m^2 kg/s^2 K) and T the absolute temperature. The prediction of the plateau modulus as inferred from the more accurate phantom network theory ($G_0 = \nu k_bT\cdot(f-2)/f$), which does take into account fluctuations of the cross-linking nodes and the resulting reduction of cumulative stretching of the network strands, approaches the affine network prediction in the limit of high cross-linking functionalities f.[91] The real elastic network theory (RENT), developed by Olsen and Johnson[92,93] as an extension of the phantom network theory, takes into account different orders of cyclic topological defects (loops), but again approximates the affine network theory at higher functionalities. Since the functionalities of micellar cross-linking nodes with aggregation numbers on the order of 50−100[26] are a priori assumed to be relatively large even if a significant fraction of loops is present, this provides a justification for the use of the affine network approach.

The fraction of the available soluble blocks that are elastically active can thus also be calculated from the plateau modulus as

$$\frac{\nu}{(a-1)\cdot n} = \frac{G_0}{(a-1)\cdot n\cdot k_bT} \tag{13}$$

Besides the generalization of the transient network model of Annable et al.[67,68] for multiblock copolymers, another novelty of our work is the fact that n_m will be experimentally determined, rather than approximated via a theoretical balance. In contrast with Annable's assumption of a randomly close-packed lattice of micellar cores,[67] our approach using Small-Angle X-ray Scattering (SAXS) characterization will provide information about the exact spatial distribution of the micellar cores, as specified by the radial distribution function $g(r)$, and will hence facilitate a better representation of the network's microstructure (see Section 4.2). Additionally, Annable and coauthors[68] argue that their assumption of a random arrangement ($g(r) = 1$) of micellar cores throughout the sample might be violated at least at concentrations close to the critical network concentration $c_{network}$, as the analysis of NMR data[94,95] showed that the structure might be fractal up until some length scale at these concentrations.[96] The approach of using experimental information about the exact radial distribution was previously suggested by Annable and co-workers[68] to improve the performance of their model, but to the best of our knowledge, it has never been implemented. Therefore, the current study combines insights from the experimentally probed network topology, resulting in

https://doi.org/10.1021/acs.macromol.2c01500
Macromolecules 2023, 56, 612−633

n_m and N_{agg} values of multiblock copolymers with known values of a and M_w, with a generalization of a mechano-statistical network model, to predict the evolution of the network elasticity as a function of concentration. In Figure 3, a schematic overview of the transient network model is given, i.e., the input, main principles, output, and verification, as well as where experimental methods come into play.

3. EXPERIMENTAL SECTION

3.1. Materials. ExpertGel (EG) polymers of type 312 and 412 were kindly donated by PolymerExpert (France) and used without further purification. ExpertGel molecules are linear multiblock copolymers of alternating poly(ethylene oxide) (PEO) and poly(propylene oxide) (PPO) blocks. They are formed by connecting PEO_x–PPO_y–PEO_x triblock copolymers (also referred to as Pluronics, a trademark of BASF) using poly(propylene glycol)-12/saturated methylene diphenyl diisocyanate (PPG-12/SMDI) copolymer, and terminated by additional PEO blocks. The links are formed by urethane chemistry between a terminal hydroxy group and the reactive isocyanate of SMDI. EG312 consists of Pluronic F108 (poloxamer 338, PEO_{141}–PPO_{44}–PEO_{141} on average), whereas EG412 consists of Pluronic F127 (poloxamer 407, PEO_{101}–PPO_{56}–PEO_{101} on average). The linking PPG-12/SMDI copolymer contains on average 4 repeating PPG-12/SMDI units. Table 2 summarizes the molecular characteristics of both types of commercially available ExpertGel, as inferred from Fourier Transform Infrared Spectroscopy (FT-IR), Gel Permeation Chromatography (GPC) and ^{1}H Nuclear Magnetic Resonance Spectroscopy (^{1}H NMR) (see Supporting Information for detailed analysis). The weight fraction of EO monomers relative to the weight of EO + PO monomers (f_{EO}) matches the values as specified by the manufacturer. The a parameter, representing the average amount of hydrophobically associating blocks per chain, is approximated based on the following formula:

Table 2. Molecular Characteristics of the Two Grades of ExpertGel (EG312 and EG412) Used in Our Study: Number Average Molecular Weight ($\overline{M_n}$), Weight Average Molecular Weight ($\overline{M_w}$), Molecular Weight Dispersity (Đ), Weight of EO Monomers Relative to the Weight of EO + PO (f_{EO}), and the Average Number of Hydrophobically Associating Blocks per Chain (a)

sample	$\overline{M_n}$ [kDa][a]	$\overline{M_w}$ [kDa][a]	Đ [−]	f_{EO} [−][b]	a [−][c]
ExpertGel 312	29	63	2.15	0.83	3.95
ExpertGel 412	23	44	1.88	0.75	3.60

[a]Determined by GPC. [b]Determined by ^{1}H NMR. [c]Calculated with eq 14.

$$a = \frac{(1 - f_{EO}) \cdot \overline{M_w}}{\overline{M_{w,PPO}}} \tag{14}$$

in which $\overline{M_{w,PPO}}$ represents the average molecular weight of the PPO blocks, i.e., the amount of repeating PO monomers in a PPO block times the molar mass of the PO monomer (58 g/mol). The amount of PO monomers (46 for EG312 and 52 for EG412) is calculated as an average between the y PO monomers of the precursor Pluronic (y = 44 for EG312 and y = 56 for EG412) and the 4 repeating PPG-12 blocks, bearing in total 48 PO monomers in the PPG-12/SMDI copolymer linker. Note that for the use of the a parameter in the binomial distribution $P(\Psi)$ around the average value $\langle\Psi\rangle$ (see Section 2 for the derivation of the mechano-statistical transient network model), the calculated values in Table 2 should be rounded to their nearest natural number, which makes the value equal to 4 for both types of ExpertGel. Based on this a value, the ExpertGel molecules consist of the following overall structure: poloxamer–PPG-12/SMDI–poloxamer–PPG-12/SMDI–PEO end-cap, bearing in total approximately 4 hydrophobic blocks.

ExpertGel aqueous solutions were prepared by dissolving the required amount of EG (accuracy of 0.01 mg) in Milli-Q water (Sartorius Arium 611DI, conductivity of 0.055 μS/cm at room temperature) by magnetic stirring in an ice bath for at least 45 min. The cold samples were left in the fridge at 4 °C for at least 12 h, to completely eliminate the foam layer. The samples were used within 1 week after preparation.

3.2. Characterization Techniques. *3.2.1. Rheometry.* Rheological measurements were performed using a stress-controlled rheometer (DHR3, TA Instruments) in strain-controlled mode. The temperature was controlled by means of a Peltier system connected to a fluid bath, with an accuracy of ±0.1 °C.

For measuring dilute, low viscous solutions of multiblock copolymers, an anodized aluminum double wall Couette (DWC) geometry was used to ensure sufficient sample response with respect to the lower torque limit of the device (5 nNm in rotation as specified by the manufacturer). The dimensions of the cup and bob are $D_{c,i}$ = 40 mm, $D_{b,i}$ = 40.76 mm, $D_{b,o}$ = 43.92 mm, $D_{c,o}$ = 44.76 mm and H_b = 60 mm (c = cup, b = bob, i = inner, o = outer). All DWC measurements were conducted at a gap of 1 mm between the bottom of the bob and the cup, but no significant influence of the gap was found in the range from 500 μm up to 1 mm. A solvent trap was used to prevent solvent evaporation. For each measurement, exactly 7.5 mL of sample was loaded in the DWC cup coming directly from the fridge at 4 °C. The sample was kept at 15 °C for a flow sweep from 1 to 100 s^{-1}, after which the sample was heated to the desired temperatures using a controlled heating rate of 0.1 °C/min, while shearing at a constant shear rate of 100 s^{-1}. At intermediate temperatures in steps of 5 °C from 20 to 50 °C, flow sweeps from 1 to 100 s^{-1} were recorded, after which the heating was continued to reach the next intermediate temperature. The Milli-Q solvent was also measured using this protocol in order to determine the solvent viscosity at each intermediate temperature as well.

For concentrated solutions, a stainless steel plate–plate (PP) geometry with a diameter of 40 mm was used. The samples were measured at a gap of 250 μm. The gap was continuously adjusted for thermal expansion in order to keep it constant, by using a thermal gap compensation value of 0.82 μm/°C. The latter was calibrated at a rate of 0.1 °C/min by consecutive zero gap determinations. The effects of possible wall slip during linear oscillatory measurements were checked by performing the measurement protocol at different gap heights (ranging from 150 to 750 μm), but no significant difference nor a decreasing trend in rheological parameters with decreasing gap could be discerned, indicating that wall slip was insignificant. To avoid solvent evaporation at elevated temperatures, a peripheral mineral oil layer was placed around the sample after scraping the excess sample and reaching the measurement gap (at low temperatures). It was kept in place by means of a metal ring with a diameter of 49 mm, glued onto the bottom plate of the rheometer. The influence of the low viscosity mineral oil (viscosity of 0.143 Pa s at 25 °C) on the rheological properties of the gel networks was found to be insignificant by comparing the response with and without oil layer during initial times at which the measurement was not yet affected by solvent evaporation. The measurement protocol was the following: after carefully loading and scraping the samples coming directly from the fridge at 4 °C, the samples were monitored under small amplitude oscillatory shear at 15 °C using a strain of 0.1% at a frequency of 1 Hz over a period of 10 min, to ensure a thermal equilibrium. Afterward, a frequency sweep from 100 to 0.01 Hz at 0.1% strain was recorded. The samples were subsequently probed with a strain of 0.1% and a frequency of 1 Hz when heating to the desired temperatures using a controlled heating rate of 0.1 °C/min. At intermediate temperatures in the range from 16 to 50 °C in steps of 2 °C, frequency sweeps from 100 to 0.01 Hz with a strain of 0.1% were recorded after which the heating was continued to reach the next intermediate temperature. The strain value of 0.1% was verified to be in the linear regime for all samples and conditions.

3.2.2. Small-Angle X-ray Scattering. Small-Angle X-ray Scattering (SAXS) measurements were performed on a commercial laboratory beamline (Xeuss 2.0C, Xenocs) consisting of a Cu K_α ultralow dispersion X-ray source (50 kV, 0.6 mA) with wavelength 1.54189 Å and a Dectris EIGER 1 M detector. The X-ray beam was collimated to a

https://doi.org/10.1021/acs.macromol.2c01500
Macromolecules 2023, 56, 612−633

Table 3. Polymer Parameters of the PEO and PPO Blocks Present in the Two Grades of ExpertGel (EG312 and EG412): the Number of Monomers n, the Molecular Weight of the Block $M_{w,b}$, the Number of Kuhn Segments N, the Kuhn Length b, and the Theoretically Predicted Radius of Gyration R_g

	PEO block					PPO block				
sample	n[a]	$M_{w,b}$ [Da][a]	N[b]	b [Å][c]	R_g [nm][d]	n[e]	$M_{w,b}$ [Da][e]	N[b]	b [Å][c]	R_g [nm][d]
ExpertGel 312	141	6204	23.64	7.25	1.44	46	2668	5.26	10.63	0.75
ExpertGel 412	101	4444	16.93	7.25	1.22	52	3016	5.95	10.63	0.79

[a]Based on the length of the PEO block in the precursor Pluronics F108 (EG312) and F127 (EG412). [b]Calculated with eq 17. [c]Calculated with eq 18. [d]Determined by eq 20 using $\nu = {}^1/_2$ for PEO and $\nu = {}^1/_3$ for PPO. [e]Calculated as an average between the PPO block of the precursor Pluronics and that of the PPG-12/SMDI copolymer linker.

diameter of 0.5 mm at the sample position. A Linkam stage (HFSX350) with a temperature accuracy <0.1 °C was used as a temperature-controlled sample holder. The entire beam path was under vacuum (<10 mbar) to reduce parasitic air scattering contributions during measurements. Calibration of the sample-to-detector distance (1.1929 m) was performed using a silver(I) behenate standard. This laboratory setup allowed to investigate a q-range of 0.006−0.255 Å^{-1}, where q represents the scattering vector defined by $q = 4\pi(\sin\theta)/\lambda$ in which 2θ is the scattering angle, thus corresponding to angles from 0.04° to 1.79°. Using Bragg's law ($q = 2\pi/d$), this q-range matches length scales from 2.5 to 105 nm.

Samples were injected in borosilicate glass capillaries with a diameter of 0.9 mm (WJM-Glas/Müller GmbH) at low temperatures, after which the capillaries were sealed using glue from a glue gun and placed in the Linkam stage at 30 °C. The samples were heated to the desired temperatures using a controlled heating rate of 0.1 °C/min. At intermediate temperatures in the range from 30 to 50 °C in steps of 2 °C, three images of 1 h acquisition time were collected at a constant temperature, after which the heating was continued to reach the next intermediate temperature. The three scattering images per sample and temperature were averaged to avoid large contributions from cosmic radiation at longer measurement times. The 2D images were radially integrated to obtain 1D scattering intensity profiles $I(q)$ using Foxtrot software (Xenocs/Synchrotron du Soleil). The measured intensities were corrected using the absolute intensity scale, taking into account the intensity of the transmitted direct beam, measured at the detector as an average prior to and post data collection. Subtraction of the Milli-Q water background was performed on the 1D intensity profiles prior to further data analysis.

The 1D data fitting was performed with SASview 5.0.3 software using the Levenberg−Marquardt fitting algorithm. A combination of a Porod power law $I_0 \cdot q^{-p}$, a spherical form factor $P(q)$ and a hard sphere structure factor $S(q)$ was fitted onto the data, according to eq 15 in which I_0 and I_{bckg} represent scaling and background intensities, respectively:

$$I(q) = I_0 \cdot q^{-p} + P(q) \cdot S(q) + I_{bckg} \tag{15}$$

The expression for the spherical form factor is given in eq 16 with r the spherical radius and $\Delta\rho = \rho_s - \rho_{sol}$ being the difference in scattering length densities for the sphere (s) and solvent (sol):

$$P(q) = 12\pi \cdot r^3 \cdot \Delta\rho^2 \cdot \left[\frac{\sin(qr) - qr\cos(qr)}{(qr)^3}\right]^2 \tag{16}$$

The hard sphere structure factor is determined by assuming a Percus−Yevick closure relation to solve the Ornstein−Zernike equation.[97] Possible polydispersity of the spherical radius was not taken into account in the fitting procedure. The scattering length density ρ_{sol} of the Milli-Q water solvent was fixed at 9.47×10^{-6} Å^{-2}. The fitting was performed in the q-range from 0.006−0.01 Å^{-1} and weighed with the errors determined by the radial integration of the 2D-images. The q-range >0.01 Å^{-1} was not taken into account due to large errors after Milli-Q solvent subtraction.

3.2.3. Data Analysis. All data analyses were performed using MATLAB 2021b, unless specified otherwise.

3.3. Polymer Parameters. The transient network elasticity of the micellar networks formed by multiblock copolymers finds its origin in the presence of soluble, hydrophilic bridges in between micellar nodes. Such bridges will only form over length scales on the order of the radius of gyration of an intermediate hydrophilic block.[98] To theoretically predict the radii of gyration of the PEO and PPO blocks in our alternating multiblock copolymers, knowledge of the number of Kuhn segments N and the Kuhn length b of the equivalent freely jointed Kuhn chains with the same characteristics as the blocks, is required. This can be calculated according to eqs 17 and 18, respectively:

$$N = \frac{M_w \cdot \cos^2\theta/2}{M_0 \cdot C_\infty} \tag{17}$$

$$b = \frac{C_\infty \cdot l}{\cos\theta/2} \tag{18}$$

in which M_w represents the molecular weight of the entire block, M_0 the molecular weight of the repeating monomer, C_∞ Flory's characteristic ratio, θ the tetrahedral angle, and l the bond length.[91] The tetrahedral angle θ for both PEO and PPO is 68°.[91] The bond length can be calculated as an arithmetic mean of the bonds present in the monomer of the polymer backbone, l(C−C) = 1.54 Å and l(C−O) = 1.43 Å,[99−101] with the second one occurring twice. The mean bond length l thus equals 1.47 Å, which is similar for PEO and PPO. The molar mass M_0 of the monomers in PEO and PPO is 44 g/mol and 58 g/mol, respectively. Flory's characteristic ratio, which is a measure of the chain's local stiffness as an ideal chain, is experimentally determined by intrinsic viscosity [η] measurements at Θ-conditions: for PEO $C_\infty = 4.1 \pm 0.4$ (H_2O + 0.45 M K_2SO_4 at 35 °C)[99] and for PPO $C_\infty = 6.01$ (isooctane at 50 °C).[102] Similar values were obtained using mass spectrometry ($C_{\infty,PEO} = 3.96$ and $C_{\infty,PPO} = 5.76$).[101] The number of monomers n, the molecular weight M_w, and the resulting values for the number of Kuhn segments N and the Kuhn length b of the average PEO and PPO blocks are summarized in Table 3.

The theoretical calculation of the size of a polymer in solution does not only depend on the Kuhn characteristics N and b, but also on the solvent quality, which is reflected in the scaling exponent ν in the Flory scaling relation $\sqrt{\langle R^2\rangle} \sim bN^\nu$.[91] It is well-known that low molecular weight polymer chains can be approximated as ideal chains ($\nu = {}^1/_2$) in the so-called Θ-region. Theoretically a chain can be treated as ideal as long as the number of Kuhn segments N is smaller than the number of monomers g_T in a thermal blob.[91] The latter can be calculated based on the Flory interaction parameter χ as

$$g_T = \frac{1}{(1 - 2\chi)^2} \tag{19}$$

The value of χ for linear PEO polymers in Milli-Q water was experimentally determined by Merrill et al. using osmotic pressure measurements and equals 0.426.[103] By equating N and g_T, a maximum molecular weight of 12 000 g/mol is obtained as the limiting PEO molecular weight for an ideal chain approximation, which justifies treating our relatively short PEO blocks (maximum 6 204 g/mol) as ideal chains. PPO chains with a M_w of 2000 g/mol are only soluble in water at low temperatures (<18 °C)[104] and hence, water is considered a nonsolvent ($\nu = {}^1/_3$) for higher molecular weight PPO at room

https://doi.org/10.1021/acs.macromol.2c01500
Macromolecules 2023, 56, 612−633

temperature. In both cases, i.e. ideal θ-conditions with $\nu = {}^1/_2$ and nonsolvent conditions with $\nu = {}^1/_3$, the radius of gyration R_g for linear flexible chains can be calculated according to eq 20:

$$R_g = \frac{b \cdot N^{\nu}}{\sqrt{6}} \tag{20}$$

The calculated sizes for the PEO and PPO blocks present in our alternating multiblock copolymers, according to this theoretical expression, are also included in Table 3.

4. RESULTS AND DISCUSSION

4.1. Critical Concentration for Network Formation. It is well-known that Pluronic triblock copolymers (PEO_x–PPO_y–PEO_x) undergo microscopic phase separation in aqueous solutions due to the dehydration of the central hydrophobic PPO block at elevated temperatures.[49,50] The critical onsets of micellization with respect to temperature and concentration, are referred to as the Critical Micelle Temperature (CMT) and the Critical Micelle Concentration (CMC), respectively, and they can be determined by different characterization techniques. Aqueous solutions of alternating multiblock copolymers of PEO and PPO with similar block lengths as their precursor Pluronics F108 and F127, also undergo micellization above a certain critical temperature. In another study,[105] we extensively investigated this entropy-driven micellization and the phase transitions as a function of temperature and concentration for both types of ExpertGel using a multitude of techniques including rheometry, calorimetry, dynamic light scattering, and light transmittance, and we compared the characteristics to that of their precursor Pluronics.

Linear oscillatory shear rheology measurements on concentrated multiblock copolymer solutions reveal an elastic contribution upon micellization, indicative of the formation of a solid-like network as a function of temperature. However, the absence of a calorimetric process other than that of the micellization, shows that no higher hierarchical, crystalline structuring takes place,[105] as is the case for Pluronics.[106] Alternatively, the alternating sequences of soluble PEO blocks capped by hydrophobic PPO blocks allow the formation of elastic PEO bridges between two different hydrophobic cores. Therefore, the network formed by alternating PEO–PPO multiblock copolymers is assumed to be constructed through hydrophobic, micellar cores connected by hydrophilic bridges.[106] This is similar to the network formation of BAB triblock copolymers bearing their hydrophobic blocks as telechelic end groups, with the difference that one multiblock copolymer can form multiple hydrophilic bridges and hence can connect more than two hydrophobic cores within the network. A schematic illustration of such network formation was previously illustrated in Figure 1. It is important to mention that the thermally induced micellization and network formation of PEO–PPO multiblock copolymers are thermoreversible, as can be inferred from rheological heating and cooling ramps (see Figure 4 for temperature ramps of a 140 g/L EG312 solution at 0.1 °C/min). Note that at this high frequency of 100 rad/s, the elastic modulus G' saturates to a constant value at high temperatures (with an increase <4% in the relevant temperature range from 40 to 46 °C).

Undoubtedly, the capability of a soluble PEO block to form an elastic bridge greatly depends on the proximity of other micellar cores. Besides a critical concentration for micelle formation at a certain temperature (CMC(T)), there thus also exists a critical temperature dependent concentration $c_{network}$ at which micellization results in the formation of bridges between micellar cores and hence a network, rather than fully isolated micelles. This concentration represents a theoretical boundary at which at least one other micellar core is close enough such that an intermediate soluble PEO block can span the distance between these two neighboring micellar cores. Upon increasing the concentration above the critical network concentration, continuously more micellar cores are in close proximity and the material transforms from a viscous Newtonian solution of isolated micelles to a viscoelastic network of bridged micellar cores. At concentrations around this critical network concentration, large fluctuations in the microstructure usually induce unstable and irreproducible behavior[11,107] and render a macroscopic, experimental assessment of $c_{network}$ in real systems very challenging. As an alternative, $c_{network}$ can be approximated from the overlap concentration c^* of the entire multiblock copolymer. This overlap concentration c^* represents the transition from the dilute to semidilute concentration regime, and is defined as the concentration at which there is exactly one polymer chain present in the volume defined by its radius of gyration R_g:

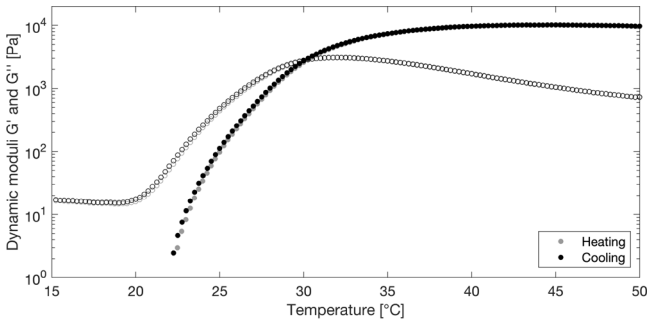

Figure 4. Dynamic moduli G' (filled circle) and G'' (unfilled circle) as a function of temperature for a 140 g/L EG312 solution during heating and cooling ramps at a rate of 0.1 °C/min, a frequency of 100 rad/s and 0.1% strain. For clarity, only 1 out of 40 consecutive data points are shown.

$$c^* = \frac{M_w}{(4\pi/3) \cdot {R_g}^3 \cdot N_{Av}} \tag{21}$$

Using c^* as an approximation for $c_{network}$ would underestimate the actual value of $c_{network}$ as it does not necessarily allow hydrophobic blocks of different polymer chains to aggregate and form a micellar core. In this regard, it is important to point out that the PEO–PPO multiblock copolymers used in this study are not end-capped by hydrophobic PPO blocks, but contain soluble PEO blocks as dangling ends. Therefore, $c_{network}$ is defined as the concentration at which one full chain plus one repeating PEO–PPO unit are present in the volume defined by the radius of gyration of the entire multiblock copolymer:

$$c_{network} = \frac{M_w + (M_w/a)}{(4\pi/3) \cdot {R_g}^3 \cdot N_{Av}} \tag{22}$$

It is relevant to mention that the hydrophobic association between PPO blocks cannot be viewed as "point interactions" due to the significant size of the PPO blocks. This definition of $c_{network}$ thus ensures that two PPO blocks from different multiblock copolymer chains can find each other and can fully overlap at the critical network concentration. Note that to determine the molecular weight of the repeating unit we have simply divided the molecular weight of the entire multiblock copolymer by the amount of repeating PEO–PPO sequences.

https://doi.org/10.1021/acs.macromol.2c01500
Macromolecules 2023, 56, 612–633

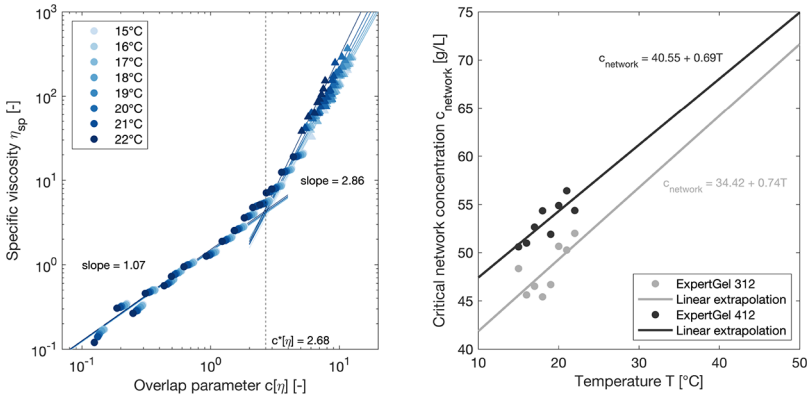

Figure 5. Viscosity scaling and determination of temperature dependent $c_{network}$: (a) specific viscosity η_{sp} versus overlap parameter $c[\eta]$ for EG312 at different low temperatures (<CMT). The lines represent the power law scalings in the dilute and semidilute regions. The overlap concentration c^* is determined at the crossover of both scaling regimes. The value of $c^*[\eta]$ and the slopes indicated in the graph are average values. (b) Critical network concentration $c_{network}$ versus temperature for EG312 and EG412. The lines represent the linear extrapolation to higher temperatures.

The latter can be approximated by using the a parameter defined as the average amount of PPO blocks per multiblock copolymer. Since the critical network concentration can thus be calculated from the overlap concentration c^* of the entire chain as

$$c_{network} = \frac{a+1}{a} \cdot c^* \tag{23}$$

an experimental assessment of c^* at multiple low temperatures below the CMT, where no micellar aggregation takes place, will enable determination of a temperature dependent $c_{network}$. Finally, it is important to stress that such definition of $c_{network}$ is hypothetical, as it decouples micellization and network formation by omitting the microstructural changes upon micellization and assuming random chain configurations upon network formation.

The critical transition from the dilute to the semidilute concentration regime at the overlap concentration c^*, is often inferred from the scaling of viscosity with concentration. Figure 5a shows the specific viscosity $\eta_{sp} = (\eta - \eta_{sol})/(\eta_{sol})$ as a function of the dimensionless concentration $c[\eta]$ for EG312 at multiple low temperatures below the CMT. The temperature dependent intrinsic viscosity $[\eta]$ is determined according to the Huggins's method, i.e. $\lim_{c\to 0} \eta sp/c$. The obtained values for the intrinsic viscosities of EG312 and EG412 at 20 °C are 67.63 mL/g and 54.15 mL/g, respectively. These values are in line with the value of 67.78 mL/g obtained for linear PEG chains of 35 000 g/mol in water at 20 °C[108] and 53.3 mL/g at 25 °C,[109] and follow the trend of increasing intrinsic viscosity with increasing molecular weight and decreasing temperature.[108] The viscosities at low concentrations, represented by the circle symbols in Figure 5a, were determined from the temperature sweeps at 100 s^{-1} using the double wall Couette geometry. Flow sweeps from 0.1 s^{-1} up to 100 s^{-1} at these temperatures show Newtonian behavior for these dilute polymer solutions. The viscosities at higher concentrations, represented by the triangle symbols, were determined from oscillatory temperature sweeps at a frequency of 1 Hz and 0.1% strain using the plate−plate geometry. Note that for purely viscous solutions with a phase angle close to 90°, which is the case at low temperatures below the CMT, the viscosity can be calculated from the loss modulus G'' and the angular frequency ω using the relationship $\eta' = G''/\omega$ and $\lim_{\omega\to 0} \eta' = \lim_{\dot{\gamma}\to 0} \eta_0$.

Changes in the slope of η_{sp} versus $c[\eta]$ in a log−log plot are linked to the critical transitions from dilute to semidilute solutions (at c^*), from semidilute unentangled to semidilute entangled (at c_e) and to concentrated solutions (at c^{**}).[110] Only one clear transition is observed in Figure 5a, with the slope changing from 1.07 to 2.86. The viscosity scaling of EG412 at multiple low temperatures below the CMT can be found in the Supporting Information (see Figure S6) and shows similar behavior with the slope changing from 1.12 at low concentrations to 3 at higher concentrations. The crossover, as an average of all probed temperatures, happens at $c^* = 2.68/[\eta]$ for EG312 and at $c^* = 2.24/[\eta]$ for EG412. The slope of 1.07 in the first region in Figure 5a is very close to 1 and corresponds to the dilute regime according to the Zimm model.[110] The slope of 2.86 in the second region is rather high as compared to the slope of $1/(3\nu - 1) = 1.3$ usually obtained for semidilute unentangled (homo)polymer solutions in good solvents ($\nu = 0.588$) and relatively low as compared to the usually obtained slope of $3/(3\nu - 1) = 3.9$ for semidilute entangled solutions in good solvents.[91] For linear PEO (with a minimum molecular weight of 100 000 g/mol) in water at 20 °C indeed a slope of 3.85 was obtained in the semidilute entangled regime.[111] We hypothesize that this intermediate slope obtained for our multiblock copolymers above c^* finds its origin in the possible weak associative interactions between PPO blocks below the CMT, which do not result in true micellar self-assembly. These short-lived interactions restrict the flow of the polymers and induce a more pronounced concentration dependence of the viscosity as compared to that of simple homopolymers. However, these interactions are less effective as the restrictions imposed by physical entanglements. Higher scaling exponents than theoretically predicted by the Rouse−Zimm model for semidilute unentangled polymers were also observed by Zhang et al. for polyimide solutions containing associative dipole−dipole interactions.[112] Finally, the c^* transition of our multiblock copolymers happens at $\eta_{sp} = 4$, meaning that the solution viscosity is roughly 5 times that of the solvent, whereas the critical transition to the semidilute entangled regime at c_e usually happens at viscosities of 10−300 times the solvent viscosity.[110] Therefore, the transition observed for our multiblock copolymers is believed to correspond to the transition from a dilute to a semidilute unentangled polymer solution at the overlap concentration c^*. The absence of another transition,

https://doi.org/10.1021/acs.macromol.2c01500
Macromolecules 2023, 56, 612−633

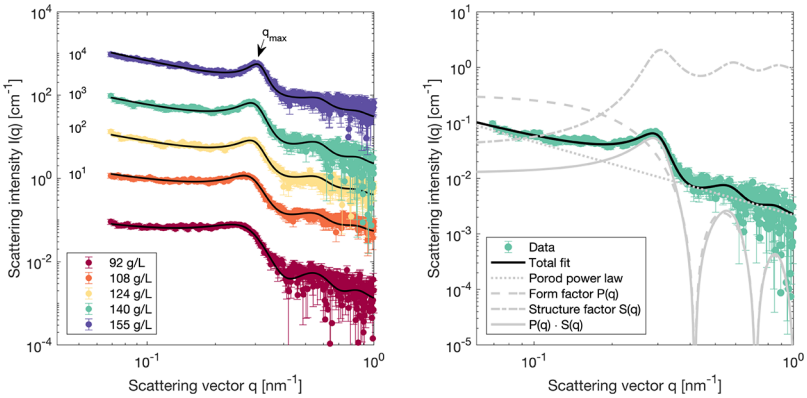

Figure 6. Small-angle X-ray scattering measurements on EG312 at 46 °C: (a) Background corrected scattering intensities $I(q)$ at different concentrations (> $c_{network}$). Shift factors are indicated on the graph. Solid lines represent curve fittings. (b) Separate fitting contributions for 140 g/L EG312 including a Porod power law, a spherical form factor $P(q)$, and a hard sphere structure factor $S(q)$.

at concentrations above c^*, indicates that our study operates in a concentration range with no entanglements between entire multiblock copolymer chains and hence also not between soluble blocks. This justifies our assumption that entanglements are not significant in the micellar networks and therefore are also not taken into account in the transient network model in Section 2. From the experimentally determined c^*, we can also get an indication of the radius of gyration R_g of the multiblock copolymer chains, resulting in 8.67 nm for EG312 at 15 °C and 7.60 nm for EG412 at 15 °C. Using the theoretically calculated radii of gyration of the separate PEO and PPO blocks (see Table 3), another approximation of the number of repeating PEO−PPO sequences in the entire multiblock copolymer can be determined. The as such calculated values of 3.97 and 3.74 for EG312 and EG412 respectively, comply quite nicely with the calculated a values in Table 2.

Figure 5b displays the calculated values of $c_{network}$ as a function of (low) temperature for EG312 and EG412. At these temperatures, the molecules are completely soluble without micellar aggregation. An increasing trend of $c_{network}$ with temperature is evident, indicative of a more collapsed chain configuration at elevated temperatures due to an increased dehydration of the molecules.[113] The trend, as observed for these low temperatures, is linearly extrapolated to obtain an estimate of $c_{network}$ at higher temperatures for which the viscosity scaling approach is compromised by micellization and network formation. Such linear extrapolation, i.e., $c^* \sim T$, is justified by the temperature evolution of the radius of gyration of a single PEO molecule as obtained by coarse-grain modeling,[114,115] which appears to follow a $R_g \sim T^{-1/3}$ trend. The extrapolated $c_{network}$ values will be used to predict the evolution of the n_m parameter, i.e., the amount of micellar nodes in the span of a soluble block, as a function of copolymer concentration at different temperatures. As explained in Section 2, n_m should equal 1 at all concentrations below $c_{network}$ to account for isolated micelles with PEO loops only ($F_2 = 1/n_m = 1$). Therefore, $c_{network}$ is an important, indirect parameter influencing the performance of the transient network model (via n_m and hence F_2), as it dictates where the onset of network formation is located. In the next section, n_m at concentrations above $c_{network}$ will be determined based on microstructural information on the micellar network topology.

4.2. Micellar Network Topology. The microstructure of the networks formed by alternating PEO−PPO multiblock copolymers in concentrated aqueous solutions consists of small-sized micellar cores connected by hydrophilic PEO bridges. The interaction between these structures and X-ray radiation used in Small-Angle X-ray Scattering (SAXS), allows to study the shape and size of the cores based on the angular dependency of the scattering intensity. Moreover, SAXS measurements also provide insights into the interactions between neighboring micellar cores and the overall network topology of the connected structure. In this regard, the structure factor $S(q)$ will appear to be of crucial importance for revealing the spatial distribution of the micellar cores and to determine the amount of micellar cores n_m close enough to allow bridging.

4.2.1. SAXS Intensity Profile. Figure 6a shows the scattered intensity I as a function of scattering vector q at 46 °C for multiple concentrated solutions of EG312 (92, 108, 124, 140, and 155 g/L). For clarity, the curves are shifted by the factor indicated in the graph. The error bars are determined by the radial integration of the 2D scattering images, and they do not represent independent measurements on different sample batches. Upon increasing the concentration, the structure peak, indicative of a recurring length scale d in the micro-structure, becomes more pronounced and shifts to higher q values, due to a more dense spatial arrangement. Using the empirically modified Bragg's law $d = 2.2\pi/q$ as determined for fluid-like ordered suspensions,[116] the average center-to-center intermicellar distance d corresponding to the maximum peak position q_{max}, decreases from 26.2 to 22.9 nm upon increasing the concentration from 92 to 155 g/L EG312. The data are fitted with a combination of a Porod power law, a spherical form factor $P(q)$ and a hard sphere structure factor $S(q)$ (see Section 3.2.2). These separate contributions are shown in Figure 6b for a solution of 140 g/L EG312 at 46 °C. The resulting fit is in good agreement with the experimental data. Similar graphs for EG412 can be found in Figure S7 in the Supporting Information.

The spherical shape of the micelles was previously inferred from Dynamic Light Scattering (DLS) measurements in which no significant rotational diffusion and hence no anisotropy was observed.[105] The use of a regular spherical form factor, rather than a more complex core−shell spherical form factor often used for micellar assemblies, can be justified by the absence of a significant secondary peak at higher scattering vector as compared to the primary peak, which would be indicative of a core−shell structure. In addition, SAXS studies on micellar assemblies with a PEO-based corona in aqueous solutions reveal

https://doi.org/10.1021/acs.macromol.2c01500
Macromolecules 2023, 56, 612−633

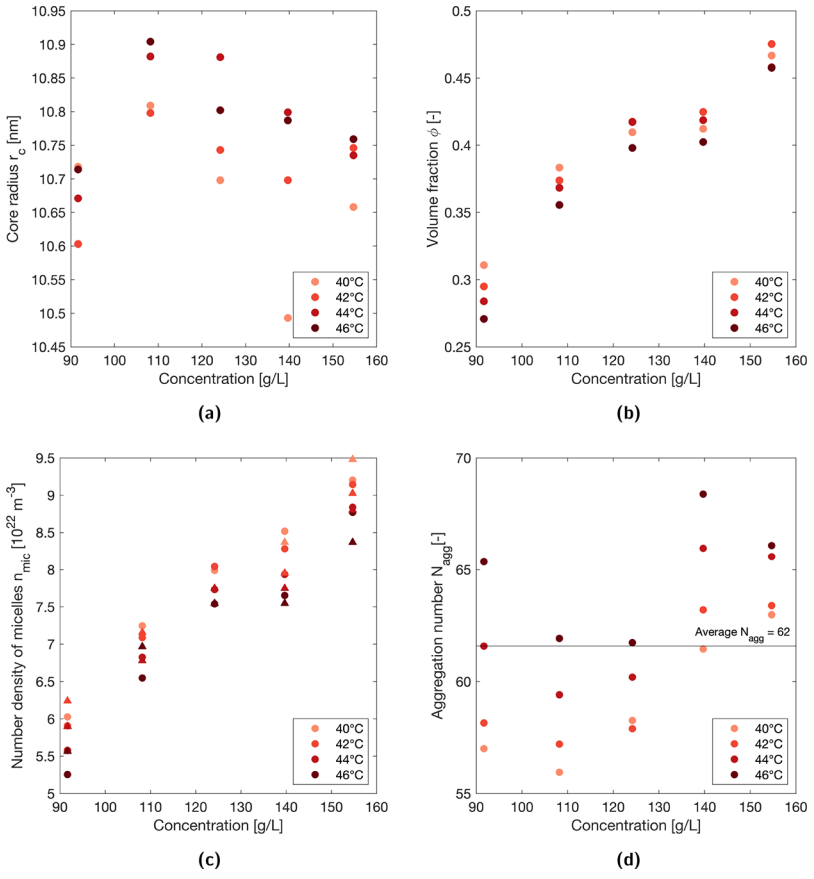

Figure 7. Evolution of the hard sphere fitting parameters (a) core radius r_c and (b) micellar volume fraction ϕ with concentration for EG312 at different temperatures (>CMT). Evolution of the calculated values (c) number density of micelles n_{mic} as calculated from SAXS fitting parameters (circles) and as calculated from $d = 2.2\pi/q_{max}$ (triangles) and (d) aggregation number N_{agg} with concentration for EG312 at different temperatures (>CMT).

that X-rays do not significantly interact with the PEO corona.[117] Hence, fitting a spherical core−shell form factor would imply that the PPO center of the micellar assemblies exists of a core and a shell with significantly different scattering length densities, other than the PEO corona. Lemmers et al.[117] used both a spherical and a core−shell form factor to describe SAXS intensity profiles of dilute micelles with a polyelectrolyte complex core and a neutral PEO corona. They found that the spherical radius obtained by using a spherical form factor equals the radius of the core plus the thickness of the shell obtained by using a core−shell approach, which indicates that a spherical radius also correctly describes the size of the overall micellar core. Since a core−shell approach would increase the amount of fitting parameters, combined with the absence of a clear fingerprint of a core−shell structure, a simple spherical form factor seems appropriate in our study. The inability to clearly detect the PEO corona with X-rays[117] implies that only the PPO cores are effectively contributing to the overall scattering intensities of the micellar networks. This supports our additional fitting assumption that the spherical radius used in the form factor ($r_{P(q)}$) and the one used in the hard sphere structure factor ($r_{S(q)}$) must be identical and equal to the PPO core size. Releasing this size constraint, i.e., $r_{P(q)} \neq r_{S(q)}$, on a selection of representative samples resulted in a difference in radius of maximum 10% between $r_{P(q)}$ and $r_{S(q)}$, with the inconsistency that for some fits $r_{P(q)} > r_{S(q)}$ was obtained, while in others the physically more plausible[117] inequality $r_{P(q)} < r_{S(q)}$ was realized. Based on these arguments, constraining the spherical radii in the form and structure factor to be equal appears reasonable. The structure factor is determined based on the Percus−Yevick closure relationship assuming no significant attractive well between individual micellar PPO cores. Only excluded volume repulsive interactions are taken into account, giving rise to a simple hard sphere approach with a micellar core radius r_c and a micellar volume fraction ϕ. For some representative samples, the use of a sticky hard sphere structure factor, to account for possible attractive interactions between the micelles, did not result in a significant attractive interaction (well depth less than kT), nor in greatly different values for r_c and ϕ, and was therefore not further considered.

As DLS indicated no significant micelle polydispersity, nor an anisotropic micellar shape,[105] the Porod power law might be induced by larger scale heterogeneities present in concentrated solutions forming networks. Such heterogeneities and the corresponding Porod law were also observed in SAXS studies on concentrated solutions of other amphiphilic molecules forming hydrophobic network nodes.[118] The obtained exponents of 1.1−1.3 for EG312 and 3.4−3.5 can be linked to mass and surface fractality, respectively, of larger scale aggregates, and further discussion hereof is beyond the scope of this work. For the curve fitting, a few other assumptions are made to reduce the amount of fitting parameters and fitting time. First, the scattering length density of the scatterer (PPO core) was forced to be larger than that of the solvent (9.47×10^{-6} Å^{-2}), as the scattering length densities of PEO and PPO were determined in the SASview software to be 10.4×10^{-6} Å^{-2} and 9.95×10^{-6} Å^{-2}, respectively. Second, with varying temperature at a specific concentration of ExpertGel, it was found that the absolute

https://doi.org/10.1021/acs.macromol.2c01500
Macromolecules 2023, 56, 612−633

intensity scale (I_0) and Porod power exponent (p) did not vary much, and hence, those were kept constant per concentration.

Parts of Figure 7a and 7b show the hard sphere fitting parameters, i.e., the radius r_c and volume fraction ϕ, respectively, as a function of EG312 concentration at different elevated temperatures above the CMT. The radius probed by SAXS (10.7 nm on average) is significantly smaller than the hydrodynamic radii (26.1 nm on average at 19 g/L EG312) obtained for dilute micelles using DLS in our other study.[105] This provides additional proof that the PEO corona is not detected using X-rays and the hard sphere radius r_c corresponds to the size of the PPO core. Upon increasing concentration, the core radius does not vary significantly, which is in contrast with the increasing hydrodynamic radius as a function of concentration for dilute solutions.[105] Nonetheless, for Pluronic PEO−PPO-PEO triblock copolymers it was also found by Static Light Scattering (SLS) and Small-Angle Neutron Scattering (SANS) studies[50,104] that the micellar size and aggregation number did not vary significantly upon increasing the concentration substantially above their CMT. The volume fraction ϕ of the micelles, on the other hand, seems to increase linearly as a function of concentration, as could be expected. Similar conclusions can be drawn for EG412 in Figure S8a,b in the Supporting Information.

From the fitting parameters r_c and ϕ, the concentration dependent number density of micelles n_{mic} can be calculated as

$$n_{mic} = \frac{\phi}{(4\pi/3)\cdot r_c^{\,3}} \tag{24}$$

Since the micellar assembly itself does not change significantly with concentration at elevated concentrations, additional copolymers are assumed to form more micelles resulting in a linearly increasing number density of micelles as a function of concentration (see circles in Figure 7c for EG312 and Figure S8c in the Supporting Information for EG412). When considering simple packing arguments, another estimate of the micellar density can be made based on the intermicellar distance d, derived from the peak maximum q_{max}, as $n_{mic} = 1/d^3$, and it is in good agreement with the values calculated from the fitting parameters (see triangles in Figure 7c for EG312 and Figure S8c in the Supporting Information for EG412). Based on the assumption that all multiblock copolymers are segregated in micellar assemblies at concentrations c above the CMC(T), an estimation of the aggregation number N_{agg} can be made according to

$$N_{agg} = \frac{a\cdot c\cdot N_{av}}{n_{mic}\cdot M_w} \tag{25}$$

in which a represents the amount of hydrophobic blocks in the multiblock copolymer and M_w the molecular weight of the multiblock copolymer. As can be seen in Figure 7d for EG312 (and Figure S8d for EG412 in the Supporting Information), the aggregation number does not change substantially with concentration nor temperature. Therefore, it will be assumed that the aggregation number, at least at these elevated concentrations, can be approximated as constant and has average values of 62 and 87 for EG312 and EG412, respectively. The maximum deviation from these values is approximately 11% for EG312 and 24% for EG412. Interestingly, by comparing the weight-average molecular weight of dilute EG312 chains at 15 °C (below CMT) with that of micelles at 45 °C (above CMT) as obtained by SLS, the aggregation number of EG312 is estimated to be 57 (see Section 3 in the Supporting Information). This nicely agrees with the value of 62 calculated from SAXS measurements on EG312 micellar networks, and justifies our calculation. Moreover, the good agreement between the aggregation numbers as determined by SLS for isolated micelles in dilute solutions and as determined by SAXS for bridged micelles in networks formed at elevated concentrations, confirms that no significant change in the micellar morphology takes place as a function of concentration. Since the scattering length density of the spherical scatterers proves that the PPO core is not completely dehydrated, an approximation of the aggregation number by simple division of the core volume ($4\pi/3\cdot r_c^{\,3}$) by the volume of the PPO block ($4\pi/3\cdot R_{g,PPO}^{\,3}$, see Table 3) represents an overestimation by approximately an order of magnitude. Instead, by taking into account a correction factor for the core volume, which accounts for the true volume of PPO in the core based on the scattering length density differences of scatterer and solvent as compared to that of PPO and solvent,[119] the obtained average aggregation numbers (143 for EG312 and 90 for EG412, see detailed calculations in Section S4 in the Supporting Information) are at least of the same order as the ones obtained from n_{mic}. Since the fitting error on the scattering length density of the core is rather small (on the order of 10^{-11} Å^{-2}), the difference between N_{agg} obtained from n_{mic} and the one obtained from r_c might be related to the oversimplification of a linear mixing rule between the scattering length densities of PPO and water in the core.

The SAXS fitting parameters r_c and ϕ, allow us to calculate the average intermicellar "gallery" spacing h, which is the distance in between the surfaces of two neighboring micellar cores by assuming a maximum separation, i.e., $d - 2r_c$, according to eq 26.

$$h = d - 2r_c = \left(\frac{1}{n_{mic}}\right)^{1/3} - 2r_c = \left(\frac{4\pi r_c^{\,3}}{3\phi}\right)^{1/3} - 2r_c = 2r_c\cdot\left[\left(\frac{\pi}{6\phi}\right)^{1/3} - 1\right] \tag{26}$$

Using the expression with r_c and ϕ, the average spacing decreases from 5.27 to 0.98 nm upon increasing the concentration from 92 to 155 g/L EG312 (at 46 °C). As compared to the radius of gyration of an intermediate soluble PEO block (in the order of 1.44 to 1.22 nm, see Table 3), this implies that the PEO blocks should, on average, stretch over approximately 3.65 times their R_g at the lowest concentration (92 g/L) to form a bridge in between two neighboring micellar cores. As this seems rather unlikely, it is anticipated that at the lowest concentration almost no bridges are formed. At the highest concentration (155 g/L), on the other hand, the average spacing is smaller than the R_g of a PEO block, thereby allowing the formation of bridges between different micellar cores. Similar conclusions can be drawn by using the distance d directly, as inferred from the maximum peak position q_{max} of the SAXS profiles in Figure 6a, resulting in an average spacing h ranging from 4.76 to 1.34 nm upon increasing the concentration from 92 to 155 g/L EG312 (at 46 °C). However, these calculations only represent an average view on the micellar spacing, and do not provide information about the local micellar distribution needed for the calculation of the crucial n_m parameter (i.e., the amount of micellar cores in such close proximity that an intermediate PEO block can form a bridge).

4.2.2. Radial Distribution Function. Fortunately, the hard sphere structure factor $S(q)$, fully defined by r_c and ϕ, can also

https://doi.org/10.1021/acs.macromol.2c01500
Macromolecules 2023, 56, 612−633

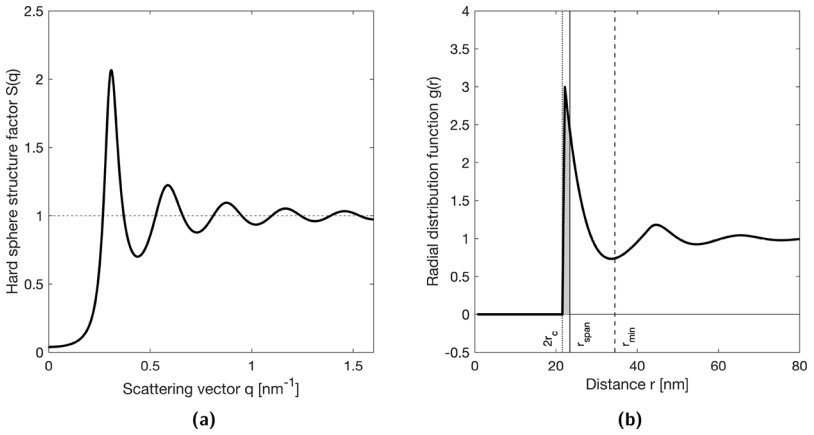

Figure 8. Determination of the amount of micellar cores n_m for 140 g/L EG312 at 46 °C: (a) the hard sphere structure factor $S(q)$ defined by r_c and ϕ and (b) the radial distribution function $g(r)$ defined by the inverse sine−Fourier transform (see eq 28) together with a Verlet−Weis correction. The spherical integration of $g(r)$ up to r_{span} (see eq 29) to determine n_m, is also indicated as the gray area under the $g(r)$ curve.

provide detailed information about the spatial distribution of micelles through its Fourier relation with the radial distribution function $g(r)$. The latter describes normalized micellar density variations around a central micellar core and reveals information about the proximity of other micelles. It can thus be used to calculate the amount of micellar cores n_m which are close enough such that an intermediate PEO block can connect to this core by forming a bridge. The relation between the structure factor $S(q)$ and the radial distribution function $g(r)$[120] is

$$S(q) = 1 + 4\pi \cdot n_{mic} \int_0^\infty r^2 \cdot [g(r) - 1] \cdot \frac{\sin(qr)}{qr}\, dr \tag{27}$$

Taking the inverse sine-Fourier transform gives the following expressing for $g(r)$:[120]

$$g(r) = 1 + \frac{1}{2\pi^2 \cdot r \cdot n_{mic}} \int_0^\infty q \cdot [S(q) - 1] \cdot \sin(qr)\, dq \tag{28}$$

It is well-known that Fourier calculations might induce artifacts, and therefore, an additional Verlet−Weis correction in the analytical Percus−Yevick solution[121] is introduced in our calculation of $g(r)$. This correction compensates the overestimation of the principal peak height in dense micellar solutions with a micellar volume fraction $\phi > 0.4$.[122] Figure 8a and 8b show the hard sphere structure factor $S(q)$ and the radial distribution function $g(r)$ calculated using the Verlet−Weis correction, respectively, for a concentrated solution of 140 g/L EG312 at 46 °C.

For the calculation of the crucial n_m parameter, a similar approach as for the calculation of the coordination number is adopted. The coordination number describes the amount of nearest neighbors and is calculated by spherical integration up until the first minimum r_{min} in the radial distribution function, thereby taking into account the first "dense" layer of micellar cores around the central core, as illustrated in the schematic in Figure 9a. Importantly, for the calculation of n_m integrating up to r_{min} would be an overestimation as intermediate PEO blocks will not necessarily be able to span the distance to all of the nearest neighbors. Therefore, the number of micellar cores in close proximity, such that a PEO block can effectively form a bridge, is calculated by integration up until a length r_{span}. The span length r_{span} is defined as twice the core radius r_c plus the radius of gyration of an intermediate PEO block $R_{g,PEO}$, which can be

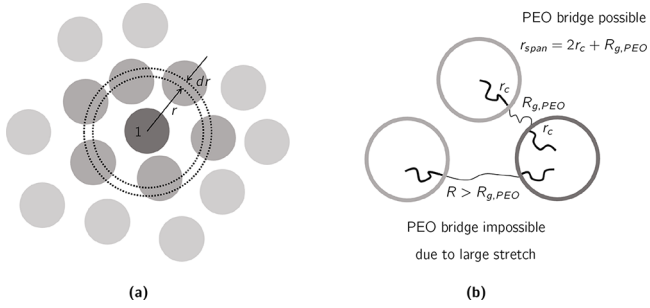

Figure 9. Schematic illustrations of (a) the radial distribution function $g(r)$ describing the normalized micellar density around a central core, represented by the dark gray core indicated with 1. The 6 nearest neighboring cores are shown as slightly lighter gray. (b) Upper right: PEO bridge between the central core (dark gray) and a neighboring core (lighter gray) over a length of $R_{g,PEO}$ with the span length defined as $r_{span} = 2r_c + R_{g,PEO}$. Lower center: impossible PEO bridge due to a too large stretch of the intermediate PEO block over a length $R > R_{g,PEO}$.

calculated with a theoretical ideal chain approximation (see Table 3). Figure 8b depicts the area under the radial distribution function $g(r)$ by integration up until r_{span}, needed for the calculation of n_m. The principle of a PEO bridge over r_{span} is illustrated in Figure 9b. The assumption that a bridge is likely to occur over a distance of R_g can be justified by the Monte Carlo simulations of Testard et al.,[98] who found that the pair potential between two colloidal particles, induced by telechelic polymer chains bridging the particles, reaches its minimum around R_g. As an approximation, we will thus assume that the main fraction of capped PEO blocks can only form a bridge toward another micellar core, instead of looping back to its own micellar core, when the other core is within an average distance of $R_{g,PEO}$. Equation 29 displays the final expression to calculate the n_m parameter:

$$n_m = 1 + 4\pi \cdot n_{mic} \int_0^{r_{span}} r^2 g(r)\, dr \tag{29}$$

Since the central micellar core (indicated as 1 in Figure 9a) is not included in the integration, one additional core is included in the calculation of n_m. Note that this central core should be reflected in n_m to ensure that without any micellar cores in close proximity, solely loops are formed with a probability $F_2 = 1/n_m = 1$. Systematically applying this formalism of converting the structure factor $S(q)$ to the radial distribution function $g(r)$,

https://doi.org/10.1021/acs.macromol.2c01500
Macromolecules 2023, 56, 612−633

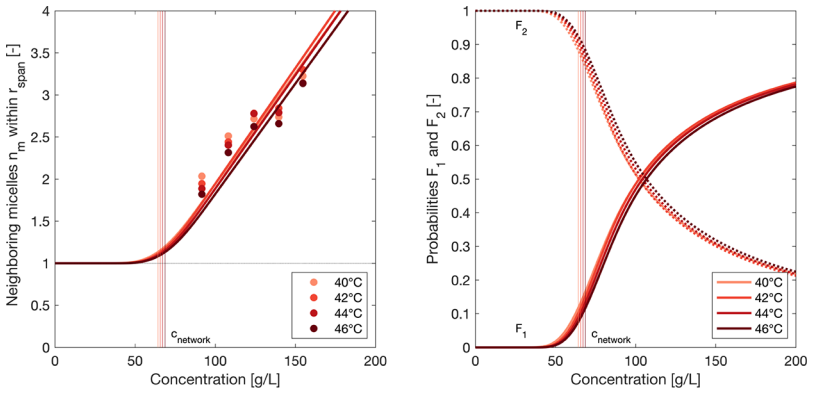

Figure 10. (a) Evolution of the experimentally determined amount of micellar cores n_m with EG312 concentration at different temperatures (>CMT). Solid lines represent fits with the additional constraint that $n_m = 1$ at $c < c_{network}$. (b) Evolution of the probabilities $F_1 = 1 - F_2$ (full line) and $F_2 = 1/n_m$ (dotted line) as a function of EG312 concentration at different temperatures (>CMT). The vertical lines on parts a and b indicate the extrapolated values of $c_{network}$ at the different temperatures.

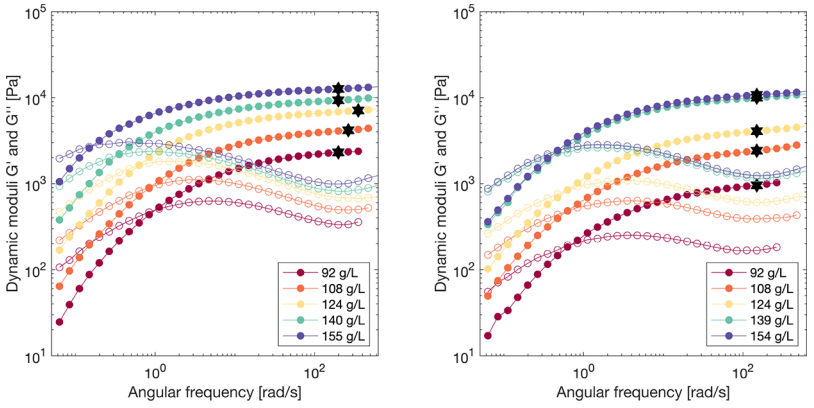

Figure 11. Dynamic moduli G' (filled symbol) and G'' (unfilled symbol) as a function of angular frequency for different concentrations ($> c_{network}$) of (a) EG312 at 46 °C and (b) EG412 at 40 °C. The black star symbols indicate the plateau modulus G_0.

followed by a spherical integration of $g(r)$ up to r_{span}, to the SAXS fitting results of micellar networks formed by EG312 or EG412 multiblock copolymers, allows one to identify a trend of n_m as a function of concentration. Figure 10a shows the evolution of the experimentally determined n_m data as a function of concentration at different temperatures for EG312, for which a clear linear trend is observed. As the probability of forming a loop F_2 is inversely related to n_m, the value of n_m is expected to be 1 (only the central core) for all concentrations below $c_{network}$. Therefore, the n_m evolution with concentration is fitted with a linear trend with the additional constraint that the linear fit should reach $n_m = 1$ at $c_{network}$. The latter was earlier determined by extrapolation of $c_{network}$ as a function of temperature (see Figure 5b) and is also indicated in Figure 10a. The final continuous evolution of n_m as a function of concentration is a combination of $n_m = 1$ at $c < c_{network}$ and the linear fit of n_m versus concentration for $c > c_{network}$, with a smooth, logistic-like transition at $c_{network}$ indicated as a solid line in Figure 10a.

The obtained concentration dependent microstructural fingerprint can directly be translated to statistical information about the micellar network topology. More specifically, the amount of micellar cores within the span length of a PEO block is linked to the probabilities F_1 and F_2 of a PEO block for either forming a bridge or a loop, respectively, through the relationships $F_2 = 1/n_m$ and $F_1 = 1 - F_2$. Figure 10b displays F_1 (solid line) and F_2 (dotted line) as a function of concentration. As expected, upon increasing concentration, the probability of forming a loop gradually decreases from 1 sufficiently below $c_{network}$ to asymptotically reaching 0 at very high concentrations (concentration $\rightarrow \infty$), while the opposite trend from 0 to 1 is observed for the probability of forming a bridge. Nonetheless, phase separation and insolubility practically limit the relevant concentration range for ExpertGel multiblock copolymers up to 200 g/L, at which F_1 and F_2 reach values of about 0.8 and 0.2, respectively. A similar, but less steep evolution was observed in the n_m values of EG412 solutions (see Figure S9a in the Supporting Information), resulting in lower probabilities for forming a bridge (Figure S9b). This can be explained by the shorter PEO block lengths and hence a smaller span width of soluble PEO blocks in networks formed by EG412. The continuous evolutions of F_1 and F_2 as a function of concentration will be used as an input for our generalized transient network model, which will be verified against experimental rheological data in the next section.

4.3. Network Elasticity and Model Performance. Dynamic rheological measurements in the linear regime, i.e., not disturbing the structure, probe the material properties at different time scales and thus provide insights in the material's overall structure. Figure 11a shows the elastic (G') and loss (G'') modulus as a function of angular frequency for different

https://doi.org/10.1021/acs.macromol.2c01500
Macromolecules 2023, 56, 612−633

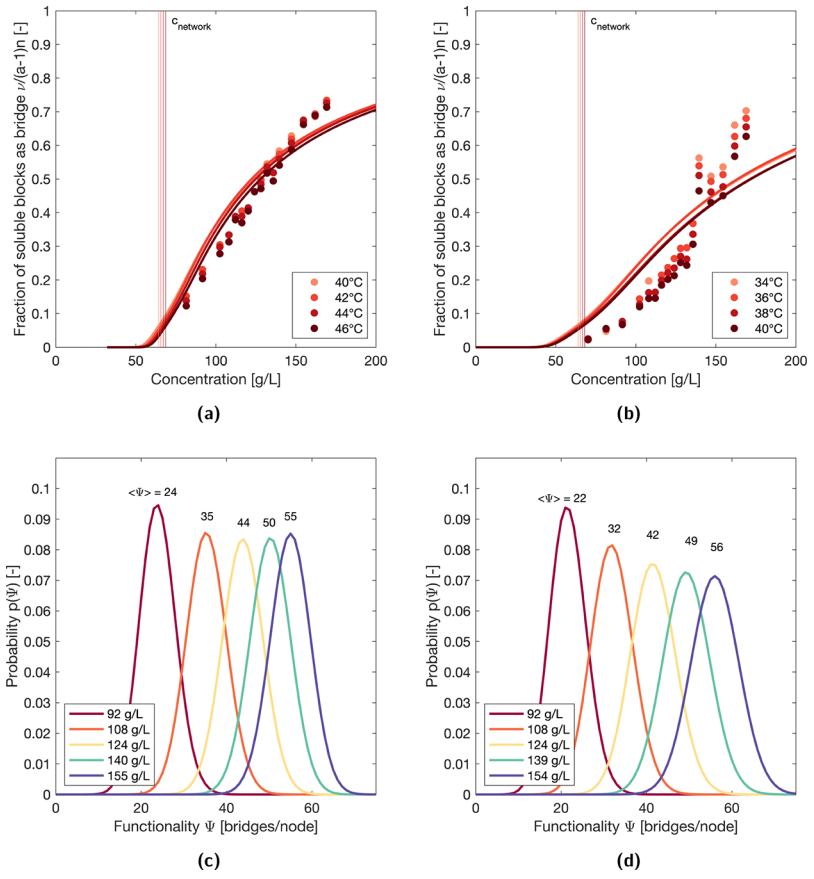

Figure 12. Fraction of soluble blocks active as a unique elastic bridge $\frac{\nu}{(a-1)n}$ as a function of (a) EG312 and (b) EG412 concentration at different temperatures (>CMT). The data symbols are calculated from the rheologically determined plateau modulus using eq 13. The solid lines represent the model predictions according to eq 11. The vertical lines indicate the extrapolated values of $c_{network}$ at the different temperatures. Probability distribution function of nodes with functionality Ψ for different concentrations ($>c_{network}$) of (c) EG312 at 46 °C and (d) EG412 at 40 °C. The distribution functions are binomial around the average ⟨Ψ⟩ (see eq 6) as indicated on the graph.

concentrations (92, 108, 124, 140, and 155 g/L) of EG312 at 46 °C. The presence of a high-frequency elastic plateau is indicative of the elastic, solid-like nature of the micellar network at short time scales. The plateau modulus G_0, defined in this work as the value of G' at the frequency at which G'' reaches its minimum[123] and indicated with black stars in Figure 11, is often used as a measure of the elasticity. Analogous to the affine network model for rubber elasticity, each elastically active strand accounts for k_BT of the elastic plateau modulus G_0 (see eq 12).[91] The terminal flow behavior ($G' \sim \omega^2$ and $G'' \sim \omega^1$) at low frequencies is proof of viscous, liquid-like behavior at longer time scales and reveals the transient character of the micellar association nodes. When given sufficient time, hydrophobic blocks detach from their micellar cores and cause the elastic bridges to relax their stored energy. The elastic plateau, relaxation process and terminal flow were also observed in the frequency sweep data of networks formed by EG412, as can be seen in Figure 11b for different concentrations of EG412 at 40 °C. Clearly, increasing the multiblock copolymer concentration results in a higher elastic modulus and a slower relaxation process, both of which can be attributed to the formation of a denser micellar network at elevated concentrations. In such a dense structure, the proximity of other micellar cores implies the formation of more elastic bridges contributing to elasticity and thereby influencing the amount of relaxation stages needed for terminal relaxation.

4.3.1. Model Performance. By performing systematic rheological measurements on networks formed by multiblock copolymers at different concentrations and temperatures, the concentration evolution of the plateau modulus G_0 can be studied (see Figure S10a,b, in the Supporting Information for EG312 and EG412, respectively). The linear evolution in the log−log plots of plateau modulus versus concentration suggests a power law scaling. Neither of the obtained exponents of 3.16 for EG312 and 4.67 for EG412 comply with the theoretically predicted power law scalings as provided by the sticky-Rouse model for unentangled, semidilute networks, e.g., $G_0 \sim \phi^{2.60}$ at low volume fractions ϕ of the polymers and $G_0 \sim \phi$ at high volume fractions in good solvents ($\nu = 0.588$ and $z = 0.225$).[76] Moreover, the concentration dependence of the plateau modulus in our micellar networks also does not obey the power law scaling relation ($G_0 \sim \phi^{0.56}$) as predicted by Semenov and Rubinstein for an unentangled micellar phase above the overlap concentration of the micelles.[87]

Due to the deviations from the existing model predictions for unentangled transient networks, the concentration evolution of $\nu/(a-1)n$ as determined by the plateau modulus (see eq 13) is compared to the prediction based on our generalized mechano-statistical transient network model (see eq 11) for EG312 in Figure 12a. The model prediction succeeds in describing the rheological data well and captures both the sharp increase at lower concentrations and the asymptotic leveling at higher

https://doi.org/10.1021/acs.macromol.2c01500
Macromolecules 2023, 56, 612−633

concentrations. Hence, the generalization of the mechano-statistical transient network model has proven to correctly predict the amount of elastically active chains as inferred from rheology. Moreover, the mechano-statistical nature of the model also enables to determine the evolution of the bridge and loop probabilities (see Figure 10b), as well as to gain insights in the node functionality probability distribution $p(\Psi)$ according to eq 6. In Figure 12c, the binomial probability distribution functions of the node functionality Ψ around its average value $\langle\Psi\rangle$ (see eq 5) are shown for different concentrations of EG312 at 46 °C. The average node functionality is more than doubled when increasing the concentration from 92 to 155 g/L EG312. Interestingly, the values of the average node functionality $\langle\Psi\rangle$ indeed show high node functionalities, even at low concentrations ($\langle\Psi\rangle$ = 24 at 92 g/L EG312), which proofs our a priori assumption of high node functionalities in micellar networks and the resulting use of the affine network approach (see Section 2).

This, together with our insights from the trends of F_1 and F_2, helps to draw a microscopic picture of the network's evolution as a function of concentration above the critical network concentration. At low concentrations, the network predominantly contains PEO loops, as $F_2 > F_1$, and the association nodes have a low functionality as compared to the overall aggregation number and the maximum number of bridges Ψ_{max}. Upon increasing the concentration, the micellar cores gradually transition into bridge-dominated, highly functional network nodes. This topological change goes hand in hand with a change in mechanical properties, reflected in both the elasticity and relaxation behavior. Similar conclusions can be drawn for EG412 networks (see model results and node probability distributions in Figure 12a and 12b, respectively).

To provide an idea about the sensitivity of the model to the SAXS fitting parameters, a sensitivity analysis by inducing a 10% variation in the core radius r_c (see Figure S11 in the Supporting Information) and in the micellar volume fraction ϕ (see Figure S12 in the Supporting Information) is performed for different concentrations of EG312 at 46 °C. The effects on the quality of the SAXS intensity profile fits (a), the crucial n_m evolution as a function of concentration (b), and the final model performance to predict the network's elasticity (c) are shown in the Supporting Information. Note that a variation in r_c and ϕ is also reflected in the aggregation number N_{agg} needed for model evaluation. A variation in the core radius r_c at constant volume fraction, on the one hand, has a pronounced effect on the quality of the SAXS profile fits, but it does not affect the n_m values as well as the model prediction significantly. A variation in the micellar volume fraction ϕ at constant core size, on the other hand, has a rather limited impact on the SAXS intensity profiles, but it does influence the n_m evolution and model predictions more severely. It can thus be concluded that the adopted approach is significantly more sensitive to the micellar volume fraction than to the micellar core size. Nonetheless, the actual elasticity data, as inferred from rheology, are located within the model boundaries induced by a 10% variation in volume fraction.

4.3.2. Critical Assessment. It must be pointed out that the model predictions for EG412 in Figure 12b are less successful in describing the concentration dependent fraction of PEO blocks active as an elastic bridge. Even though the model predicts a correct evolution of the fraction of elastically active PEO blocks, its absolute values present an overprediction at low concentrations and an underprediction at high concentrations. These over- and underpredictions of the elasticity data are also present for EG312 samples in Figure 12a, albeit to a lesser extent. Therefore, a critical assessment of the physics included in the model allows pinpointing some mechanisms not accounted for in the presented generalized mechano-statistical transient network model.

First, the presence of some odd chain configurations, which are not taken into account in the model derivation, might result in both the over- and underprediction of the elasticity. In this regard, it was previously indicated that so-called redundant bridges (see Figure 13a for a schematic representation) are not

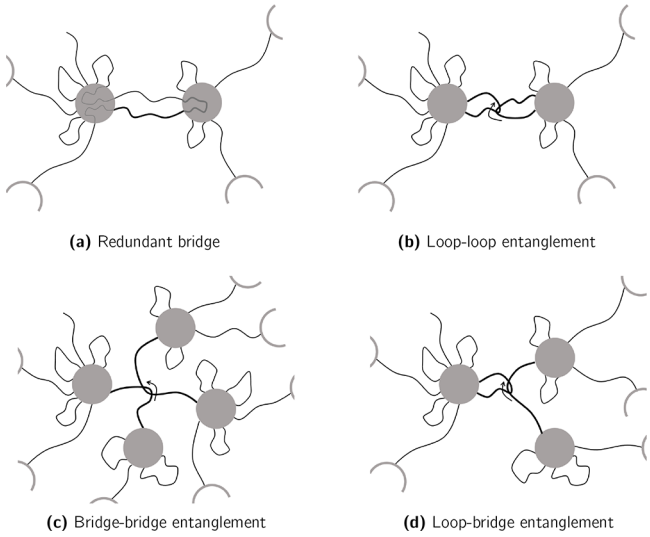

Figure 13. Schematic illustrations of (a) a redundant bridge, (b) a loop−loop entanglement, (c) a bridge−bridge entanglement, and (d) a loop−bridge entanglement. For simplicity, the micellar cores are represented as filled gray circles. The arrows indicate the entangled structure.

expected to be formed for our multiblock copolymers with relatively low a values. Nevertheless, the network structure at low concentrations close to $c_{network}$ is potentially fractal[96] and prone to fluctuations, thereby sometimes resulting in no other possibility for a chain than to revisit an old core and hence to form a redundant PEO bridge within the same chain, with a "shared" PPO block between both bridges. The presence of such redundant bridges at lower concentrations could thus possibly explain the overprediction of the elasticity by the model. Moreover, at low concentrations close to $c_{network}$, the presence of large, unconnected clusters is also not fully accounted for in our model derivations. In this regard, an extension and generalization of the mean field approach,[124] as adopted by Skrzeszewska et al.[125] for telechelic stickers undergoing trifunctional associative interactions, to multiblock copolymers with functionalities (much) higher than 3, could also possibly correct the overprediction at low concentrations. At high concentrations, on the other hand, a dense micellar structure is formed in which the chances of finding another micellar core are greatly increased. This crowded structure in turn might lead to possible "entanglements" between loops of different micellar cores (loop−loop entanglement in Figure 13b), between nonredundant bridges (bridge−bridge entanglement in Figure 13c) or between a loop and a bridge of different micellar cores (loop−bridge entanglement in Figure 13d). Note that such "entangled" configurations are solely induced by the drastic microstructural changes upon micellization at high concentrations and cannot be treated according to the classic

https://doi.org/10.1021/acs.macromol.2c01500
Macromolecules 2023, 56, 612−633

interpretation of entanglements in polymer solutions. Nonetheless, just like conventional entanglements, they do contribute to the elasticity of the network as cross-linking nodes creating additional bridges (1 extra bridge for each loop−loop entanglement and 2 extra bridges for each bridge−bridge or loop−bridge entanglement). These additional bridges are not considered in the model derivation and could provide an explanation for the underprediction of the model at elevated concentrations. The overprediction due to redundant bridges at low concentration as well as the underprediction due to entanglements at higher concentration, could both be captured in a factor α. By dividing the elasticity data as inferred from the plateau modulus (eq 13) by the model prediction (eq 11), a concentration dependent α can be obtained. Note that such ratio should be smaller than 1 at low concentrations above $c_{network}$ and larger than 1 at higher concentrations. The evolution of α as a function of concentration is shown in Figure S13a,b, in the Supporting Information for EG312 and EG412, respectively. The ratio shows that indeed the model prediction approaches the actual elasticity data for EG312 (α = 0.80−1.15), while for EG412 α ranges from 0.30 at the lowest concentration up to 1.40 at the highest concentrations. Provided that the above-mentioned configurations are the sole contributors to the over- and underprediction, it implies that at the lowest concentration of EG412 for each effective elastic bridge, there are about 2 redundant bridges, while at the highest concentration for each 5 bridges between cross-linking nodes, 2 additional bridges are created via entanglements (either as 1 bridge−bridge or loop−bridge entanglement, or as 2 loop−loop entanglements).

Second, a rather crucial parameter in the indirect evaluation of the model is the critical concentration for network formation $c_{network}$. As already mentioned, experimentally assessing this onset of network formation is often troublesome,[11,107] and rheological measurements indeed showed irreproducibility and unstable behavior of multiblock copolymer solutions at concentrations close to $c_{network}$. Therefore, we opted for an approximation of $c_{network}$ based on the overlap concentration c^* obtained from viscosity measurements (at low temperatures) in which entire multiblock copolymer chains were allowed to overlap with $1/a$th of another chain. The $(a + 1)/a$ factor serves as a correction factor, as the presence of PEO end blocks in ExpertGel molecules is also reflected in the overlap concentration c^*, thereby hindering PPO blocks of different chains to find each other at c^*. More importantly, such an approximation of $c_{network}$ assumes no microstructural change of the polymer solution upon network formation. The entropy-driven clustering of the PPO blocks, however, causes the formation of a compact hydrophobic core and hence a significantly different and more collapsed chain configuration. It is thus plausible that the theoretical approximation of $c_{network}$ from c^* represents an absolute lower limit for the critical onset concentration of networks formed by micellar aggregation.

Last, it is important to point out that the current verification is performed using commercially available systems. As a result, some polydispersity in terms of the total molecular weight as well as the length of the individual PEO and PPO blocks cannot be excluded. The overall architecture of the molecules as alternating, linear block copolymer can also be disturbed due to potential local branching induced by a very minor fraction of biuret or allophalate bonding units. However, these were not observed in the FT-IR spectra of the ExpertGel molecules (see Supporting Information). In addition, possible impurities such as PEO−PPO diblock fractions were found to be present in the precursor Pluronics[126] and affect ExpertGel as well (see GPC characterization in the Supporting Information). All of these effects have their consequences on the correct determination of M_w, a, N_{agg}, and n_m, which all need to be known a priori for model evaluation. Therefore, in the future the model should be validated with more well-defined and carefully synthesized multiblock copolymers with hydrophobic blocks distributed along the chain or even for transient polymer networks formed by multifunctional association interactions other than micellar self-assembly.

5. CONCLUSION

In this paper, we report an extension and generalization of the mechano-statistical transient network model originally developed by Annable et al.[67,68] for telechelic, hydrophobically associating triblock copolymers to more general alternating multiblock copolymers bearing multiple hydrophobic blocks along their polymer backbone. This was achieved by adopting a combinatorics approach taking into account the different configurations of loops and bridges in multiblock copolymers with multiple association blocks per chain. Herein, the probabilities of individual soluble blocks to form either a bridge (F_1) between two different association nodes or a loop ($F_2 = 1 - F_1$) toward the same association node were closely linked to the micellar network's microstructure. The loop probability F_2 was approximated as the inverse of the amount of micellar nodes n_m present within the span volume defined by a soluble, hydrophilic block. The average node functionality, defined as the average amount of bridges starting from one association node, was then determined by assessing both the average amount of bridges and the average amount of associating blocks a certain chain configuration contributes to an association node. Through the construction of a probability distribution function around this average functionality, the model enabled us to translate microstructural changes (via n_m) to statistical changes in the chain configurations (via F_1 and F_2) and eventually to macroscopic elasticity fully governed by the amount of bridges. As such, unifunctional dangling ends, as well as redundant bifunctional nodes contributing to superloops and superbridges, were eliminated in the determination of the network's elasticity. By a priori knowledge of the multiblock copolymer architecture (number of hydrophobic blocks a and M_w), as well as the micellar network structure (n_m and aggregation number N_{agg}), a complete model evaluation is possible.

For the verification of our model's performance, two grades of commercially available, alternating PEO−PPO multiblock copolymers (ExpertGel 312 and 412) forming transient micellar networks at elevated temperatures, were investigated. Rather than theoretically approaching the crucial microstructural parameters n_m and N_{agg}, they were experimentally determined by Small-Angle X-ray Scattering (SAXS) measurements. To unravel the exact spatial arrangement of the micellar nodes throughout the network, the structure factor as inferred from SAXS on concentrated solutions, was converted to the radial distribution function by its inverse Fourier relation. This allowed the determination of n_m by spherical integration of the radial distribution function up to some length scale r_{span}, defined by the radius of gyration of a soluble, hydrophilic PEO block. By combining the evolution of the experimentally determined n_m values as a function of concentration with the additional constraint that n_m equals 1 below the critical network concentration $c_{network}$, a smooth evolution of n_m with

https://doi.org/10.1021/acs.macromol.2c01500
Macromolecules 2023, 56, 612−633

concentration could be used as an input for our mechano-statistical transient network model. The critical onset concentration $c_{network}$ was determined from the overlap concentration of the multiblock copolymer solutions at low temperatures, by considering an overlap of $1/a$th of the chain.

The model predictions of the fraction of PEO blocks active as a unique elastic bridge were verified with the results inferred from linear oscillatory rheological measurements. The agreement between the model and the experimental data was within reasonable accuracy. Possible explanations of the under- and overpredictions of the network's elasticity could be found in the presence of redundant bridges at low concentrations and entangled loops and/or bridges at higher concentrations, respectively, which were not considered in the model. Nonetheless, with the help of our model a microscopic picture of the evolution of the network's topology as a function of concentration, could be derived. Below $c_{network}$, only isolated flowerlike micelles are formed without any connecting bridges, resulting in a viscous micellar solution. At concentrations slightly above $c_{network}$, loops are still predominant and the micellar nodes have rather low functionalities, leading to limited network elasticity. Upon increasing concentrations, a denser micellar arrangement induces progressively more bridges, such that bridge-dominated and highly functional network nodes are obtained. The elasticity of the ensuing network is greatly increased as compared to networks formed by lower concentrations of multiblock copolymers.

This thorough understanding of the network topology, the related statistical probabilities of bridge or loop formation, and their effect on the macroscopic rheological properties of the networks are believed to contribute to a more controlled development of physical hydrogels and transient networks in general with tailor-made mechanical properties. Moreover, our generalized mechano-statistical transient network model is believed to be useful for other equally spaced, multisticker associating polymers forming networks by multifunctional interactions.

■ ASSOCIATED CONTENT

Supporting Information

The Supporting Information is available free of charge at https://pubs.acs.org/doi/10.1021/acs.macromol.2c01500.

Section S1, generalized mechano-statistical transient network model for telechelic (triblock) copolymers; Section S2, experimental verification of the structure of the multiblock copolymers by FT-IR, GPC, and ^{1}H NMR; Section S3, static light scattering; Section S4, approximation of the aggregation number based on the core volume; and Section S5, additional figures discussed in the text (PDF)

■ AUTHOR INFORMATION

Corresponding Author

Ruth Cardinaels − *Soft Matter, Rheology and Technology, Department of Chemical Engineering, KU Leuven, 3001 Leuven, Belgium; Processing and Performance of Materials, Department of Mechanical Engineering, TU Eindhoven, 5600 Eindhoven, The Netherlands;* orcid.org/0000-0002-4191-6504; Email: ruth.cardinaels@kuleuven.be

Authors

An-Sofie Huysecom − *Soft Matter, Rheology and Technology, Department of Chemical Engineering, KU Leuven, 3001 Leuven, Belgium;* orcid.org/0000-0001-6894-4313

Wim Thielemans − *Sustainable Materials Lab, Department of Chemical Engineering, KU Leuven, campus Kulak Kortrijk, 8500 Kortrijk, Belgium;* orcid.org/0000-0003-4451-1964

Paula Moldenaers − *Soft Matter, Rheology and Technology, Department of Chemical Engineering, KU Leuven, 3001 Leuven, Belgium;* orcid.org/0000-0003-4197-2626

Complete contact information is available at: https://pubs.acs.org/10.1021/acs.macromol.2c01500

Notes

The authors declare no competing financial interest.

■ ACKNOWLEDGMENTS

The authors thank the Research Foundation Flanders (FWO) for providing An-Sofie Huysecom with a Ph.D. fellowship for fundamental research with file numbers 1180319N and 1180321N. The authors also thank Charles-André Fustin (Bio and Soft Matter, Institute of Condensed Matter and Nanoscience, UCLouvain, Belgium) for the use of GPC and ^{1}H NMR, as well as Koen Binnemans (Laboratory of Metallurgical Chemistry, Division Molecular Design and Synthesis, Department of Chemistry, KU Leuven, Belgium) for the use of FT-IR, all used for the characterization of the alternating multiblock copolymers. Finally, the authors sincerely thank PolymerExpert (France) for donating the ExpertGel samples.

■ REFERENCES

(1) Dankers, P. Y.; Hermans, T. M.; Baughman, T. W.; Kamikawa, Y.; Kieltyka, R. E.; Bastings, M. M.; Janssen, H. M.; Sommerdijk, N. A.; Larsen, A.; Van Luyn, M. J.; Bosman, A. W.; Popa, E. R.; Fytas, G.; Meijer, E. W. Hierarchical formation of supramolecular transient networks in water: A modular injectable delivery system. *Adv. Mater.* **2012**, *24*, 2703−2709.

(2) Kieltyka, R. E.; Pape, A. C.; Albertazzi, L.; Nakano, Y.; Bastings, M. M.; Voets, I. K.; Dankers, P. Y.; Meijer, E. W. Mesoscale modulation of supramolecular ureidopyrimidinone-based poly(ethylene glycol) transient networks in water. *J. Am. Chem. Soc.* **2013**, *135*, 11159−11164.

(3) Guo, M.; Pitet, L. M.; Wyss, H. M.; Vos, M.; Dankers, P. Y.; Meijer, E. W. Tough stimuli-responsive supramolecular hydrogels with hydrogen-bonding network junctions. *J. Am. Chem. Soc.* **2014**, *136*, 6969−6977.

(4) Gao, H.; Wang, N.; Hu, X.; Nan, W.; Han, Y.; Liu, W. Double hydrogen-bonding pH-sensitive hydrogels retaining high-strengths over a wide pH range. *Macromol. Rapid Commun.* **2013**, *34*, 63−68.

(5) Hu, X.; Vatankhah-Varnoosfaderani, M.; Zhou, J.; Li, Q.; Sheiko, S. S. Weak hydrogen bonding enables hard, strong, tough and elastic hydrogels. *Adv. Mater.* **2015**, *27*, 6899−6905.

(6) Cohen Stuart, M. A.; Hofs, B.; Voets, I. K.; De Keizer, A. Assembly of polyelectrolyte-containing block copolymers in aqueous media. *Curr. Opin. Colloid Interface Sci.* **2005**, *10*, 30−36.

(7) Lemmers, M.; Sprakel, J.; Voets, I. K.; Van Der Gucht, J.; Cohen Stuart, M. A. Multiresponsive reversible gels based on chargedriven assembly. *Angewandte Chemie - International Edition* **2010**, *49*, 708−711.

(8) Hunt, J. N.; Feldman, K. E.; Lynd, N. A.; Deek, J.; Campos, L. M.; Spruell, J. M.; Hernandez, B. M.; Kramer, E. J.; Hawker, C. J. Tunable, high modulus hydrogels driven by ionic coacervation. *Adv. Mater.* **2011**, *23*, 2327−2331.

(9) Menyo, M. S.; Hawker, C. J.; Waite, J. H. Versatile tuning of supramolecular hydrogels through metal complexation of oxidation-resistant catechol-inspired ligands. *Soft Matter* **2013**, *9*, 10314−10323.

(10) Jochum, F. D.; Brassinne, J.; Fustin, C. A.; Gohy, J. F. Metallo-supramolecular hydrogels based on copolymers bearing terpyridine side-chain ligands. *Soft Matter* **2013**, *9*, 2314−2320.
(11) Rossow, T.; Habicht, A.; Seiffert, S. Relaxation and dynamics in transient polymer model networks. *Macromolecules* **2014**, *47*, 6473−6482.
(12) Chen, G.; Jiang, M. Cyclodextrin-based inclusion complexation bridging supramolecular chemistry and macromolecular self-assembly. *Chem. Soc. Rev.* **2011**, *40*, 2254−2266.
(13) Liu, G.; Yuan, Q.; Hollett, G.; Zhao, W.; Kang, Y.; Wu, J. Cyclodextrin-based host-guest supramolecular hydrogel and its application in biomedical fields. *Polym. Chem.* **2018**, *9*, 3436−3449.
(14) Seiffert, S.; Sprakel, J. Physical chemistry of supramolecular polymer networks. *Chem. Soc. Rev.* **2012**, *41*, 909−930.
(15) Tuncaboylu, D. C.; Sari, M.; Oppermann, W.; Okay, O. Tough and self-healing hydrogels formed via hydrophobic interactions. *Macromolecules* **2011**, *44*, 4997−5005.
(16) Jeon, I.; Cui, J.; Illeperuma, W. R.; Aizenberg, J.; Vlassak, J. J. Extremely stretchable and fast self-healing hydrogels. *Adv. Mater.* **2016**, *28*, 4678−4683.
(17) Fan, L.; Ge, X.; Qian, Y.; Wei, M.; Zhang, Z.; Yuan, W. E.; Ouyang, Y. Advances in synthesis and applications of self-healing hydrogels. *Frontiers in Bioengineering and Biotechnology* **2020**, *8*, 1−14.
(18) Tsitsilianis, C. Responsive reversible hydrogels from associative "smart" macromolecules. *Soft Matter* **2010**, *6*, 2372−2388.
(19) Hoque, J.; Sangaj, N.; Varghese, S. Stimuli-responsive supramolecular hydrogels and their applications in regenerative medicine. *Macromol. Biosci.* **2019**, *19*, 1800259.
(20) Shang, J.; Le, X.; Zhang, J.; Chen, T.; Theato, P. Trends in polymeric shape memory hydrogels and hydrogel actuators. *Polym. Chem.* **2019**, *10*, 1036−1055.
(21) Dong, L.; Jiang, H. Autonomous microfluidics with stimuli-responsive hydrogels. *Soft Matter* **2007**, *3*, 1223−1230.
(22) Su, E.; Yurtsever, M.; Okay, O. A self-healing and highly stretchable polyelectrolyte hydrogel via cooperative hydrogen bonding as a superabsorbent polymer. *Macromolecules* **2019**, *52*, 3257−3267.
(23) Hilt, J. Z.; Gupta, A. K.; Bashir, R.; Peppas, N. A. Ultrasensitive biomens sensors based on microcantilevers patterned with environmentally responsive hydrogels. *Biomed. Microdevices* **2003**, *5*, 177−184.
(24) Park, N.; Kim, J. Hydrogel-based artificial muscles: overview and recent progress. *Advanced Intelligent Systems* **2020**, *2*, 1900135.
(25) Alexandridis, P. Amphiphilic copolymers and their applications. *Curr. Opin. Colloid Interface Sci.* **1996**, *1*, 490−501.
(26) Alexandridis, P., Lindman, B., Eds. *Amphiphilic Block Copolymers*; Woodhead Publishing Limited: Amsterdam, 2000; DOI: 10.1016/B978-0-444-82441-7.X5000-2.
(27) Chassenieux, C.; Nicolai, T.; Benyahia, L. Rheology of associative polymer solutions. *Curr. Opin. Colloid Interface Sci.* **2011**, *16*, 18−26.
(28) Eghbali, E.; Colombani, O.; Drechsler, M.; Müller, A. H.; Hoffmann, H. Rheology and phase behavior of poly(n-butyl acrylate)-block-poly(acrylic acid) in aqueous solution. *Langmuir* **2006**, *22*, 4766−4776.
(29) Ogura, M.; Tokuda, H.; Imabayashi, S. I.; Watanabe, M. Preparation and solution behavior of a thermoresponsive diblock copolymer of poly(ethyl glycidyl ether) and poly(ethylene oxide). *Langmuir* **2007**, *23*, 9429−9434.
(30) Madsen, J.; Armes, S. P. (Meth)acrylic stimulus-responsive block copolymer hydrogels. *Soft Matter* **2012**, *8*, 592−605.
(31) Li, C.; Buurma, N. J.; Haq, I.; Turner, C.; Armes, S. P.; Castelletto, V.; Hamley, I. W.; Lewis, A. L. Synthesis and characterization of biocompatible, thermoresponsive ABC and ABA triblock copolymer gelators. *Langmuir* **2005**, *21*, 11026−11033.
(32) Castelletto, V.; Hamley, I. W.; Yuan, X. F.; Kelarakis, A.; Booth, C. Structure and rheology of aqueous micellar solutions and gels formed from an associative poly(oxybutylene)-poly(oxyethylene)-poly(oxybutylene) triblock copolymer. *Soft Matter* **2005**, *1*, 138−145.
(33) Bae, S. J.; Suh, J. M.; Sohn, Y. S.; Bae, Y. H.; Kim, S. W.; Jeong, B. Thermogelling poly(caprolactone-6-ethylene glycol-b-caprolactone) aqueous solutions. *Macromolecules* **2005**, *38*, 5260−5265.
(34) Sanabria-DeLong, N.; Agrawal, S. K.; Bhatia, S. R.; Tew, G. N. Impact of synthetic technique on PLA-PEO-PLA physical hydrogel properties. *Macromolecules* **2007**, *40*, 7864−7873.
(35) Agrawal, S. K.; Sanabria-DeLong, N.; Tew, G. N.; Bhatia, S. R. Structural characterization of PLA-PEO-PLA solutions and hydrogels: Crystalline vs amorphous PLA domains. *Macromolecules* **2008**, *41*, 1774−1784.
(36) Zhang, K.; Xue, K.; Loh, X. J. Thermo-responsive hydrogels: From recent progress to biomedical applications. *Gels* **2021**, *7*, 77.
(37) Haag, R. Supramolecular drug-delivery systems based on polymeric core-shell architectures. *Angewandte Chemie - International Edition* **2004**, *43*, 278−282.
(38) Gong, C.; Qi, T.; Wei, X.; Qu, Y.; Wu, Q.; Luo, F.; Qian, Z. Thermosensitive polymeric hydrogels as drug delivery systems. *Curr. Med. Chem.* **2012**, *20*, 79−94.
(39) Stile, R. A.; Burghardt, W. R.; Healy, K. E. Synthesis and characterization of injectable poly(N-isopropylacrylamide)-based hydrogels that support tissue formation in vitro. *Macromolecules* **1999**, *32*, 7370−7379.
(40) Park, J. S.; Woo, D. G.; Sun, B. K.; Chung, H. M.; Im, S. J.; Choi, Y. M.; Park, K.; Huh, K. M.; Park, K. H. In vitro and in vivo test of PEG/PCL-based hydrogel scaffold for cell delivery application. *J. Controlled Release* **2007**, *124*, 51−59.
(41) Zhou, T.; Li, X.; Li, G.; Tian, T.; Lin, S.; Shi, S.; Liao, J.; Cai, X.; Lin, Y. Injectable and thermosensitive TGF-β1-loaded PCEC hydrogel system for in vivo cartilage repair. *Sci. Rep.* **2017**, *7*, 1−13.
(42) Liu, H.; Cheng, Y.; Chen, J.; Chang, F.; Wang, J.; Ding, J.; Chen, X. Component effect of stem cell-loaded thermosensitive polypeptide hydrogels on cartilage repair. *Acta Biomaterialia* **2018**, *73*, 103−111.
(43) Zhu, S.; Li, S.; Escuin-Ordinas, H.; Dimatteo, R.; Xi, W.; Ribas, A.; Segura, T. Accelerated wound healing by injectable star poly(ethylene glycol)-b-poly(propylene sulfide) scaffolds loaded with poorly water-soluble drugs. *J. Controlled Release* **2018**, *282*, 156−165.
(44) Zhang, J.; Zhang, M.; Lin, R.; Yun, S.; Du, Y.; Wang, L.; Yao, Q.; Zannettino, A.; Zhang, H. Allogeneic primary mesenchymal stem/stromal cell aggregates within poly(N-isopropylacrylamide-co-acrylic acid) hydrogel for osteochondral regeneration. *Applied Materials Today* **2020**, *18*, 100487.
(45) Chen, Y.; Li, Y.; Shen, W.; Li, K.; Yu, L.; Chen, Q.; Ding, J. Controlled release of liraglutide using thermogelling polymers in treatment of diabetes. *Sci. Rep.* **2016**, *6*, 1−13.
(46) Xue, K.; Zhao, X.; Zhang, Z.; Qiu, B.; Tan, Q. S. W.; Ong, K. H.; Liu, Z.; Parikh, B. H.; Barathi, V. A.; Yu, W.; Wang, X.; Lingam, G.; Hunziker, W.; Su, X.; Loh, X. J. Sustained delivery of anti-VEGFs from thermogel depots inhibits angiogenesis without the need for multiple injections. *Biomaterials Science* **2019**, *7*, 4603−4614.
(47) Gupta, M. K.; Martin, J. R.; Werfel, T. A.; Shen, T.; Page, J. M.; Duvall, C. L. Cell protective, ABC triblock polymer-based thermoresponsive hydrogels with ROS-triggered degradation and drug release. *J. Am. Chem. Soc.* **2014**, *136*, 14896−14902.
(48) Alexandridis, P.; Alan Hatton, T. Poly(ethylene oxide)poly(propylene oxide)poly(ethylene oxide) block copolymer surfactants in aqueous solutions and at interfaces: thermodynamics, structure, dynamics, and modeling. *Colloids Surf., A* **1995**, *96*, 1−46.
(49) Alexandridis, P.; Holzwarth, J. F.; Hatton, T. A. Micellization of poly(ethylene oxide)-poly(propylene oxide)-poly(ethylene oxide) triblock copolymers in aqueous solutions: thermodynamics of copolymer association. *Macromolecules* **1994**, *27*, 2414−2425.
(50) Wanka, G.; Hoffmann, H.; Ulbricht, W. Phase diagrams and aggregation behavior of poly(oxyethylene)-polyoxypropylene)-poly(oxyethylene) triblock copolymers in aqueous solutions. *Macromolecules* **1994**, *27*, 4145−4159.
(51) Pitto-Barry, A.; Barry, N. P. Pluronic® block-copolymers in medicine: From chemical and biological versatility to rationalisation and clinical advances. *Polym. Chem.* **2014**, *5*, 3291−3297.
(52) Bodratti, A. M.; Alexandridis, P. Amphiphilic block copolymers in drug delivery: advances in formulation structure and performance. *Expert Opinion on Drug Delivery* **2018**, *15*, 1085−1104.

(53) Green, M. S.; Tobolsky, A. V. A new approach to the theory of relaxing polymeric media. *J. Chem. Phys.* **1946**, *14*, 80−92.
(54) Yamamoto, M. The visco-elastic properties of network structure I. General formalism. *J. Phys. Soc. Jpn.* **1956**, *11*, 413−421.
(55) Lodge, A. S. A network theory of flow birefringence and stress in concentrated polymer solutions. *Trans. Faraday Soc.* **1956**, *52*, 120−130.
(56) Tanaka, F.; Edwards, S. F. Viscoelastic properties of physically cross-linked networks. Transient network theory. *Macromolecules* **1992**, *25*, 1516−1523.
(57) Tanaka, F.; Edwards, S. F. Viscoelastic properties of physically crosslinked networks. Part 1. Non-linear stationary viscoelasticity. *J. Non-Newtonian Fluid Mech.* **1992**, *43*, 247−271.
(58) Tanaka, F.; Edwards, S. Viscoelastic properties of physically crosslinked networks. *J. Non-Newtonian Fluid Mech.* **1992**, *43*, 289−309.
(59) Tanaka, F.; Edwards, S. F. Viscoelastic properties of physically crosslinked networks. Part 3. Time-dependent phenomena. *J. Non-Newtonian Fluid Mech.* **1992**, *43*, 289−309.
(60) Marrucci, G.; Bhargava, S.; Cooper, S. Models of shear-thickening behavior in physically cross-linked networks. *Macromolecules* **1993**, *26*, 6483−6488.
(61) Vaccaro, A.; Marrucci, G. A model for the nonlinear rheology of associating polymers. *J. Non-Newtonian Fluid Mech.* **2000**, *92*, 261−273.
(62) Tripathi, A.; Tam, K. C.; McKinley, G. H. Rheology and dynamics of associative polymers in shear and extension: Theory and experiments. *Macromolecules* **2006**, *39*, 1981−1999.
(63) van den Brule, B. H.; Hoogerbrugge, P. J. Brownian Dynamics simulation of reversible polymeric networks. *J. Non-Newtonian Fluid Mech.* **1995**, *60*, 303−334.
(64) Ng, W. K.; Tam, K. C.; Jenkins, R. D. Lifetime and network relaxation time of a HEUR-C20 associative polymer system. *J. Rheol.* **2000**, *44*, 137−147.
(65) Pellens, L.; Gamez Corrales, R.; Mewis, J. General nonlinear rheological behavior of associative polymers. *J. Rheol.* **2004**, *48*, 379−393.
(66) Pellens, L.; Ahn, K. H.; Lee, S. J.; Mewis, J. Evaluation of a transient network model for telechelic associative polymers. *J. Non-Newtonian Fluid Mech.* **2004**, *121*, 87−100.
(67) Annable, T.; Buscall, R.; Ettelaie, R.; Whittlestone, D. The rheology of solutions of associating polymers: Comparison of experimental behavior with transient network theory. *J. Rheol.* **1993**, *37*, 695−726.
(68) Annable, T.; Buscall, R.; Ettelaie, R. Network formation and its consequences for the physical behaviour of associating polymers in solution. *Colloids Surf., A* **1996**, *112*, 97−116.
(69) Golkaram, M.; Loos, K. A critical approach to polymer dynamics in supramolecular polymers. *Macromolecules* **2019**, *52*, 9427−9444.
(70) Wientjes, R. H. W.; Jongschaap, R. J. J.; Duits, M. H. G.; Mellema, J. A new transient network model for associative polymer networks. *J. Rheol.* **1999**, *43*, 375−391.
(71) Jongschaap, R. J.; Wientjes, R. H.; Duits, M. H.; Mellema, J. Generalized transient network model for associative polymer networks. *Macromolecules* **2001**, *34*, 1031−1038.
(72) Indei, T.; Takimoto, J. I. Linear viscoelastic properties of transient networks formed by associating polymers with multiple stickers. *J. Chem. Phys.* **2010**, *133*, 194902.
(73) Groot, R. D.; Agterof, W. G. Monte Carlo study of associative polymer networks. II. Rheologic aspects. *J. Chem. Phys.* **1994**, *100*, 1657−1664.
(74) Groot, R. D.; Agterof, W. G. Dynamic Viscoelastic Modulus of Associative Polymer Networks: Off-Lattice Simulations, Theory and Comparison to Experiments. *Macromolecules* **1995**, *28*, 6284−6295.
(75) Semenov, A. N.; Rubinstein, M. Thermoreversible gelation in solutions of associative polymers. 1. Statics. *Macromolecules* **1998**, *31*, 1373−1385.
(76) Rubinstein, M.; Semenov, A. N. Thermoreversible gelation in solutions of associative polymers. 2. Linear dynamics. *Macromolecules* **1998**, *31*, 1386−1397.
(77) Leibler, L.; Rubinstein, M.; Colby, R. H. Dynamics of reversible networks. *Macromolecules* **1991**, *24*, 4701−4707.
(78) Rubinstein, M.; Semenov, A. N. Dynamics of entangled solutions of associating polymers. *Macromolecules* **2001**, *34*, 1058−1068.
(79) Feldman, K. E.; Kade, M. J.; Meijer, E. W.; Hawker, C. J.; Kramer, E. J. Model transient networks from strongly hydrogen-bonded polymers. *Macromolecules* **2009**, *42*, 9072−9081.
(80) Xu, D.; Craig, S. L. Scaling laws in supramolecular polymer networks. *Macromolecules* **2011**, *44*, 5465−5472.
(81) Hackelbusch, S.; Rossow, T.; van Assenbergh, P.; Seiffert, S. Chain dynamics in supramolecular polymer networks. *Macromolecules* **2013**, *46*, 6273.
(82) Verjans, J.; André, A.; Van Ruymbeke, E.; Hoogenboom, R. Physically Cross-Linked Polybutadiene by Quadruple Hydrogen Bonding through Side-Chain Incorporation of Ureidopyrimidinone with Branched Alkyl Side Chains. *Macromolecules* **2022**, *55*, 928−941.
(83) Regalado, E. J.; Selb, J.; Candau, F. Viscoelastic behavior of semidilute solutions of multisticker polymer chains. *Macromolecules* **1999**, *32*, 8580−8588.
(84) Cram, S. L.; Brown, H. R.; Spinks, G. M.; Hourdet, D.; Creton, C. Hydrophobically modified dimethylacrylamide synthesis and rheological behavior. *Macromolecules* **2005**, *38*, 2981−2989.
(85) Kujawa, P.; Audibert-Hayet, A.; Selb, J.; Candau, F. Effect of ionic strength on the rheological properties of multisticker associative polyelectrolytes. *Macromolecules* **2006**, *39*, 384−392.
(86) Semenov, A. N.; Joanny, J. F.; Khokhlov, A. R. Associating polymers: Equilibrium and linear viscoelasticity. *Macromolecules* **1995**, *28*, 1066−1075.
(87) Semenov, A. N.; Rubinstein, M. Dynamics of entangled associating polymers with large aggregates. *Macromolecules* **2002**, *35*, 4821−4837.
(88) Mordvinkin, A.; Döhler, D.; Binder, W. H.; Colby, R. H.; Saalwächter, K. Terminal flow of cluster-forming supramolecular polymer networks: Single-chain relaxation or micelle reorganization? *Phys. Rev. Lett.* **2020**, *125*, 127801.
(89) Mordvinkin, A.; Döhler, D.; Binder, W. H.; Colby, R. H.; Saalwächter, K. Rheology, sticky chain and sticker dynamics of supramolecular elastomers based on cluster-forming telechelic linear and star polymers. *Macromolecules* **2021**, *54*, 5065−5076.
(90) Jangizehi, A.; Ahmadi, M.; Seiffert, S. Emergence, evidence, and effect of junction clustering in supramolecular polymer materials. *Materials Advances* **2021**, *2*, 1425−1453.
(91) Rubinstein, M.; Colby, R. H.*Polymer Physics*; Oxford University Press: Oxford, U.K., 2003.
(92) Wang, R.; Alexander-Katz, A.; Johnson, J. A.; Olsen, B. D. Universal cyclic topology in polymer networks. *Phys. Rev. Lett.* **2016**, *116*, 1−5.
(93) Zhong, M.; Wang, R.; Kawamoto, K.; Olsen, B. D.; Johnson, J. A. Quantifying the impact of molecular defects on polymer network elasticity. *Science* **2016**, *353*, 1264−1268.
(94) Nyström, B.; Walderhaug, H.; Hansen, F. K. Dynamic crossover effects observed in solutions of a hydrophobically associating water-soluble polymer. *J. Phys. Chem.* **1993**, *97*, 7743−7752.
(95) Walderhaug, H.; Hansen, F. K.; Abrahmsén, S.; Persson, K.; Stilbs, P. Associative thickeners. NMR self-diffusion and rheology studies of aqueous solutions of hydrophobically modified poly-(oxyethylene) polymers. *J. Phys. Chem.* **1993**, *97*, 8336−8342.
(96) Annable, T.; Buscall, R.; Ettelaie, R.; Shepherd, P.; Whittlestone, D. Influence of Surfactants on the Rheology of Associating Polymers in Solution. *Langmuir* **1994**, *10*, 1060−1070.
(97) Percus, J. K.; Yevick, G. J. Analysis of Classical Statistical Mechanics by Means of Collective Coordinates. *Phys. Rev.* **1958**, *110*, 1−13.
(98) Testard, V.; Oberdisse, J.; Ligoure, C. Monte Carlo simulations of colloidal pair potential induced by telechelic polymers: Statistics of loops and bridges. *Macromolecules* **2008**, *41*, 7219−7226.
(99) Flory, P. J.; Mark, J. E. The configuration of the polyoxyethylene chain. *J. Am. Chem. Soc.* **1965**, *87*, 1415−1423.

https://doi.org/10.1021/acs.macromol.2c01500
Macromolecules 2023, 56, 612−633

(100) Abe, A.; Hirano, T.; Tsuruta, T. Conformational energies and the random-coil configuration of poly(oxypropylene). *Macromolecules* **1979**, *12*, 1092−1100.
(101) Kokubo, S.; Vana, P. Easy access to the characteristic ratio of polymers using Ion-Mobility Mass Spectrometry. *Macromol. Chem. Phys.* **2017**, *218*, 1600373.
(102) Allen, G.; Booth, C.; Price, C. III-The unperturbed dimensions of poly(propylene oxide). *Polymer* **1967**, *8*, 397−401.
(103) Merrill, E. W.; Dennison, K. A.; Sung, C. Partitioning and diffusion of solutes in hydrogels of poly(ethylene oxide). *Biomaterials* **1993**, *14*, 1117−1126.
(104) Mortensen, K.; Pedersen, J. S. Structural study on the micelle formation of poly(ethylene oxide)−poly(propylene oxide)−poly-(ethylene oxide) triblock copolymer in aqueous solution. *Macromolecules* **1993**, *26*, 805−812.
(105) Huysecom, A.-S.; Glorieux, C.; Thoen, J.; Thielemans, W.; Fustin, C.-A.; Moldenaers, P.; Cardinaels, R.Phase behavior of medium-length hydrophobically associating PEO-PPO multiblock copolymers in aqueous media. Submitted, 2022.
(106) Pham Trong, L. C.; Djabourov, M.; Ponton, A. Mechanisms of micellization and rheology of PEO-PPO-PEO triblock copolymers with various architectures. *J. Colloid Interface Sci.* **2008**, *328*, 278−287.
(107) Grindy, S. C.; Lenz, M.; Holten-Andersen, N. Engineering elasticity and relaxation time in metal-coordinate cross-linked hydrogels. *Macromolecules* **2016**, *49*, 8306−8312.
(108) Abdel-Azim, A. A. A.; Atta, A. M.; Farahat, M. S.; Boutros, W. Y. Determination of intrinsic viscosity of polymeric compounds through a single specific viscosity measurement. *Polymer* **1998**, *39*, 6827−6833.
(109) Kashmola, T. O.; Kamil, E. S. Structure rheology of polyethylene oxide solution. *Iraqi Journal of Chemical and Petroleum Engineering* **2014**, *15*, 23−32.
(110) Colby, R. H. Structure and linear viscoelasticity of flexible polymer solutions: Comparison of polyelectrolyte and neutral polymer solutions. *Rheol. Acta* **2010**, *49*, 425−442.
(111) Ebagninin, K. W.; Benchabane, A.; Bekkour, K. Rheological characterization of poly(ethylene oxide) solutions of different molecular weights. *J. Colloid Interface Sci.* **2009**, *336*, 360−367.
(112) Zhang, E.; Dai, X.; Dong, Z.; Qiu, X.; Ji, X. Critical concentration and scaling exponents of one soluble polyimide - From dilute to semidilute entangled solutions. *Polymer* **2016**, *84*, 275−285.
(113) Su, Y. L.; Liu, H. Z.; Wang, J.; Chen, J. Y. Study of salt effects on the micellization of PEO-PPO-PEO block copolymer in aqueous solution by FTIR spectroscopy. *Langmuir* **2002**, *18*, 865−871.
(114) Chudoba, R.; Heyda, J.; Dzubiella, J. Temperature-Dependent Implicit-Solvent Model of Polyethylene Glycol in Aqueous Solution. *J. Chem. Theory Comput.* **2017**, *13*, 6317−6327.
(115) Raubenolt, B.; Gyawali, G.; Tang, W.; Wong, K. S.; Rick, S. W. Coarse-grained simulations of aqueous thermoresponsive polyethers. *Polymers* **2018**, *10*, 475.
(116) Liu, J.; Schöpe, H. J.; Palberg, T. An improved empirical relation to determine the particle number density of fluid-like ordered charge-stabilized suspensions. *Particle and Particle Systems Characterization* **2000**, *17*, 206−212.
(117) Lemmers, M.; Voets, I. K.; Cohen Stuart, M. A.; Der Gucht, J. V. Transient network topology of interconnected polyelectrolyte complex micelles. *Soft Matter* **2011**, *7*, 1378−1389.
(118) Zhang, X.; Kyriakos, K.; Rikkou-Kalourkoti, M.; Kitiri, E. N.; Patrickios, C. S.; Papadakis, C. M. Amphiphilic single and double networks: a small-angle X-ray scattering investigation. *Colloid Polym. Sci.* **2016**, *294*, 1027−1036.
(119) Puig-Rigall, J.; Obregon-Gomez, I.; Monreal-Pérez, P.; Radulescu, A.; Blanco-Prieto, M. J.; Dreiss, C. A.; González-Gaitano, G. Phase behaviour, micellar structure and linear rheology of tetrablock copolymer Tetronic 908. *J. Colloid Interface Sci.* **2018**, *524*, 42−51.
(120) Yarnell, J. L.; Katz, M. J.; Wenzel, R. G.; Koenig, S. H. Structure factor and radial distribution function for liquid argon at 85 Â°K. *Phys. Rev. A* **1973**, *7*, 2130−2144.
(121) Verlet, L.; Weis, J. J. Equilibrium theory of simple liquids. *Phys. Rev. A* **1972**, *5*, 939−952.
(122) Riest, J.; Eckert, T.; Richtering, W.; Nägele, G. Dynamics of suspensions of hydrodynamically structured particles: Analytic theory and applications to experiments. *Soft Matter* **2015**, *11*, 2821−2843.
(123) Liu, C.; He, J.; van Ruymbeke, E.; Keunings, R.; Bailly, C. Evaluation of different methods for the determination of the plateau modulus and the entanglement molecular weight. *Polymer* **2006**, *47*, 4461−4479.
(124) Case, L. C. Branching in polymers. I. Network defects. *J. Polym. Sci.* **1960**, *45*, 397−404.
(125) Skrzeszewska, P. J.; De Wolf, F. A.; Werten, M. W.; Moers, A. P.; Cohen Stuart, M. A.; Van Der Gucht, J. Physical gels of telechelic triblock copolymers with precisely defined junction multiplicity. *Soft Matter* **2009**, *5*, 2057−2062.
(126) Mortensen, K.; Batsberg, W.; Hvidt, S. Effects of PEO-PPO diblock impurities on the cubic structure of aqueous PEO-PPO-PEO pluronics micelles: Fee and bcc ordered structures in F127. *Macromolecules* **2008**, *41*, 1720−1727.

https://doi.org/10.1021/acs.macromol.2c01500
Macromolecules 2023, 56, 612−633